Modelling the mediation of treatment effects on prion fibril aggregation by intrinsic fibril breakage parameters

Author: Jens de Groot

Student number: S3396428

Supervisors: Sander van Doorn and Ulrich Eisel

Research group: Theoretical Research in Evolutionary Life Sciences (TRÊS)

Date: October 2023

Abstract

Protein aggregation is a key phenomenon in neurodegenerative diseases. Since decades, researchers attempted to capture the dynamics of prion protein propagation with mathematical models. Key mechanisms of protein propagation are elongation of misfolded protein aggregates by the recruitment of monomers and, accordingly, breakage into daughter filaments that can elongate again. It is especially these breakage mechanisms that are important to model. An increasing body of research shows that the breakage rate of linear protein aggregates follows a non-linear relationship with fibril length. Next, it is proposed that the breakage rate depends on the position along which a fibril breaks. Furthermore, there are several treatment options that can be incorporated into a mathematical model, such as chaperones and interferons. The combination of these is important, because different breakage mechanisms may modulate the effect of treatments in different ways. The current study tries to separately implement both length and position-dependent breakage parameters combined with chaperones or interferons as treatment options into a predictive model. We find that a moderate length-dependent breakage or breakage at the center contributes most to measures of (pathogenic) protein fibril propagation. The results are discussed in light of empirical results and clinical practice.

Content

Introduction

Prion diseases or transmissible spongiform encephalopathies (TSE) and amyloid-related neurological diseases are neurodegenerative diseases that are always fatal. Several attempts have been made to better understand the dynamics of these diseases. These dynamics are often described with the nucleation-polymerization model. Although there are multiple types of protein aggregates (see review of Balchin, Hayer-Hartl, & Hartl, 2016), we focus here on linear aggregates that grow in one direction. These are the so-called fibrillar aggregates or filaments. In essence, the dynamics are that two or more misfolded protein molecules form a nucleus. This nucleus then 'infects' healthy proteins and hence elongates. The infectious fibrils that arise may then break to form more infectious fibrils (Garzón et al., 2021; Masel, Jansen, & Nowak, 1999). Besides biomolecular research (Abdelaziz, Abdulrahman, Gilch, & Schatzl, 2019; Kawahara, Kato-Negishi, & Tanaka, 2021) there is the computational field of research on protein aggregation.

The latter field is concerned with generating mathematical models in order to better understand mechanisms behind protein aggregation. To date, multiple studies have tried to capture the population dynamics of the interaction of the normal endogenous prion protein (PrP^{C}) with its misfolded, infectious and protease-resistant variant (PrP^{Sc}). This was often done in combination with practical experiments. In this article, I first give a state-of-the-art overview of the literature on the dynamics of (infective) protein fibril aggregation. In this review, I focus on literature that addressed the nucleated polymerization model of protein fibril aggregation. Next, I come up with a model that combines aspects of multiple articles on protein fibril aggregation. This model includes several aspects of breakage and treatment. The set up is to validate this model and assess the separate influences of breakage mechanisms and treatments on protein aggregation dynamics. After that, the interaction between breakage mechanisms and treatment is tested.

Review of the literature

The nucleated polymerization model and first uses

The nucleated polymerization model is a model to describe the aggregation of common, misfolded prion or amyloid proteins. In essence, the first step that is assumed to happen is the nucleation step. This is a step in which two or more (infectious) protein monomers bind together to form a dimer or oligomer. This small aggregate can then form polymers with other monomers. The polymers make the monomers misfold and aggregate with them. In this way the protein aggregate grows bigger. Eventually, it can break into two shorter aggregates that can elongate again. In this way, protein fibers duplicate and the population of fibers can grow. The first studies that assessed the dynamics of protein aggregation with a nucleated polymerization population model for prions were the studies of Nowak, Krakauer, Klug and May (1998) and Masel, Jansen and Nowak (1999). In their research, they made use of a nucleated polymerization model. According to this model, incoming monomeric susceptible normal cellular prion protein (PrP^{C}) can be converted to prion protein scrapie (PrP^{Sc}) after interaction with polymeric PrP^{Sc}. In this way, an infectious PrP^{Sc} polymer is able to elongate with a constant rate (Masel et al., 1999; Nowak et al., 1998). In a later phase, the PrP^{Sc} polymers break into smaller polymers with a certain rate and the process of elongation is repeated. The breakage rate was assumed to be independent of polymer length. In their model, they did allow for some degradation of PrP^{Sc}. In order to mimic resistance to degradation (Silveira et al., 2005; Weber et al., 2007), this degradation rate was

determined much smaller than the natural degradation rate of PrP^C (Masel et al., 1999; Nowak et al., 1998). The resulting theoretical distribution of polymer length was right skewed, showing that smaller lengths dominated in their simulated sample (Masel et al., 1999; Nowak et al., 1998). Furthermore, with help of their model, Masel and colleagues could estimate the reproductive ratio R_0 of several prion protein strains. Here, R_0 is a measure for how efficient prions can propagate throughout their environment (the brain). The higher R_0 is, the more efficient prions can propagate. An R_0 below 1 causes misfolded prions to extinct, whereas an R_0 above 1 causes misfolded prions to propagate and accumulate (Masel et al., 1999).

Statistical aspects of protein fibril aggregation

The theoretical results of these and other works concur partly with empirical chemical findings on proliferation of (PrP^{Sc}) fibrils (Masel et al., 1999; Nowak et al., 1998; Rubenstein et al., 2007). For example, it was shown that denaturized PrP^C formed aggregates following a certain right-skewed length distribution (Prigent et al., 2014). Several other empirical studies showed the same phenomenon. For instance, with the help of atomic force microscopy it was found that the length of amyloid fibrils could be described with a log-normal distribution (Baldwin et al., 2008; Morris et al., 2013; Sorci, Grassucci, Hahn, Frank, & Belfort, 2009), an exponential distribution (van Raaij, van Gestel, Segers-Nolten, de Leeuw, & Vinod Subramaniam, 2008) or with a right-skewed Weibull distribution (Arosio, Beeg, Nicoud, & Morbidelli, 2012; Sorci, Silkworth, Gehan, & Belfort, 2011; Xue & Radford, 2013; Xue, Homans, & Radford, 2009).

Time dynamics of protein fibril aggregation

While the above paragraph describes a statistical aspect of protein aggregation, there are several dynamic aspects of aggregation as well. Firstly, theoretical protein aggregation models are able to describe a logistic decay and growth of monomers and polymers (aggregates), respectively (Nowak et al., 1998; Greer, Pujo-Menjouet, & Webb, 2006; Greer, van den Driessche, Wange, & Webb, 2007; Rubenstein et al., 2007). And indeed, with fluorescence microscopy, it could be observed that the population of free monomers mimicked a logistic decay curve over time (Shvadchak, Claessens, & Subramaniam, 2015). Conversely, it could be shown that the population of the protein polymers over time followed a logistic growth curve (Alvarez-Martinez et al., 2011; Collins, Douglass, Vale, & Weissman, 2004; Marchante et al., 2017; Nicoud, Lazzari, Barragán, & Morbidelli, 2015; Xue & Radford, 2013). Secondly, theoretical models show that the mean length of (prion) protein fibrils over time follows a biphasic trajectory. Initially, the mean length increases drastically before it gradually comes to a hold. After this, it decreases until a stable equilibrium length is reached (Arosio, Beeg et al., 2012; Greer et al., 2006; Nowak et al., 1998). Experimental results also confirm this. An explanation for this is that fibrils become more prone to break as they grow. This gives rise to a phase in which elongation of fibrils is more prominent. What follows is the phase in which breakage is more prominent as a consequence of elongation (Arosio, Beeg et al., 2012; Nicoud et al., 2015; Schreck & Yuan; 2013; Xue & Radford, 2013).

Uses of protein aggregation model assumptions in theoretical research

As with every theoretical model, protein aggregation models do have some particular assumptions that may lead to limitations. Below, we list common model assumptions and describe their relevance.

After that, the assumptions are validated against findings from empirical studies. Some often used model assumptions include:

1) The breakage rate is constant or linearly dependent on the length of the protein fibril;
2) The likelihood of breakage is independent of the position of the breakage;
3) The intrinsic elongation rate above a critical size is constant;
4) Degradation rate
5) Fibril-fibril association

Note that assumptions 1) and 2) are tightly connected to each other, assumption 2) implies assumption 1). In the model of Masel and colleagues (1999), it was assumed that the likelihood of a breakage of the fibril to occur is independent on the site in the fibril. This means that the fragmentation rate of infectious protein fibrils is linearly dependent on the fibril length. Since then, this type of modelling had been replicated in other publications (Davis and Sindi, 2015; Morris et al., 2013; Engler, Prüss, & Webb, 2006; Prüss, Pujo-Menjouet, Webb, & Zacher, 2006). A limitation of this assumption is that it requires modelers to implement a set of equations for each fibril length, as the fragmentation rate differs per fibril length. This can eventually lead to a situation in which there is an infinite number of differential equations to be solved. Garzón et al. (2021) used a constant fragmentation rate for all fibril lengths to overcome this problem, which leads to a system with a finite number of equations. This virtually means that each protein fibril has only one breakage site and is equally likely to break. In this way, a model would not be able to capture any relationship between fibril length and breakage rate. Another solution is to model the fibril length as a continuous variable. With this, both the linear length-dependence and mathematical tractability can be retained (Greer et al., 2006, 2007; Engler et al., 2006; Prüss et al., 2006). The third assumption is that there is a constant elongation rate (Arosio, Beeg et al., 2012; Davis & Sindi; Engler et al., 2006; Garzón et al., 2021; Greer et al., 2006, 2007; Masel et al., 1999; Nicoud et al., 2015; Nowak et al., 1998; Prüss et al., 2006; Schreck & Yuan, 2013). There are, however, few studies that take into account a polymer length-dependent elongation rate (Calvez et al., 2009, 2010). These assumptions are advantageous in the sense that they are simpler to implement in a model. However, such assumptions in their simplicity can lead to theoretical results that differ from empirical findings.

Model assumption 1

First of all, while most models assume a linear-dependent breakage rate of protein fibrils, empirical data suggest differently. In an article of Beal et al., (2020), it turned out that empirical data on fibril fragmentation showed non-linear relationships between breakage rate and fibril length. In contrast to other models, the model in this study allowed for a more general relationship between breakage rate and fibril length, a so-called power law:

$$B(x) \propto x^{\gamma} \quad (1);$$

where x is the length of the fibril (be it discrete or continuous). A value of $\gamma = 1$ would mean that the relationship between fiber breakage rate and length is linear. However, it was found that mean values of γ varied between 1.7 and 5.7, depending on the protein strain. Obviously, these values imply a non-linear relationship (Beal et al., 2020; Xue and Radford, 2013). Other studies found that a value near $\gamma = 3$ fitted their data (Arosio, Beeg et al., 2012; Collins et al., 2004). Others found a length-dependent

relationship that was also strain-dependent, but did not specify the value for the exponent in the power law (Nicoud et al., 2015). Hence, it is important in this research to take into account the value of the power in relationship (1). The assumption of a mere linear relationship may also be too simplistic. This is also important from a biological perspective. Namely, recently it was implied that the power law in (1) influences the length distribution of the protein fibril population (Beal et al., 2020). It was also shown that infectivity of fibrils was length dependent (Silveira et al., 2005). Therefore, assumptions on the power law may also have implications for the biological infectivity of the (theoretical) protein fibril population. Thus, an overly simplistic relationship may give wrong estimates for the infectivity of the fibril population and possibly also for treatment potentials.

Model assumption 2

Secondly, empirical results with regard to the breakage location in relation with the likelihood of the breakage are in concordance with results on relationship (1). The non-linear relationship between fibril length and breakage rate was repeatedly accompanied by a site-dependent likelihood of breakage of the fibril. It was observed that this site-dependent likelihood was also dependent on the protein strain. Some strains were more likely to break in the middle (centrally), whereas other strains had a higher chance of breaking at the end (i.e., by eroding) (Nicoud et al., 2015). In one study, it could be observed that, the higher the value of γ, the more likely it was for a protein fibril to break in the center (Beal et al., 2020). Therefore, we can conclude that assumption 2) may be too simplistic for our predictive model. We pay further attention to *assumption 2* in this work.

Model assumption 3

Thirdly, one can make assumptions about the intrinsic elongation rate as well, based on empirical data. With the intrinsic elongation rate, we mean the elongation rate of a fibril irrespective of external influences, such as the concentration of monomers. However, the way in which assumption 3) can be reviewed is a bit less straightforward. Next to resistance to digestion by proteinase kinase there is the converting activity that indicates the potential infectivity of a prion protein fibril. It is thought that this converting activity is a measure of the elongation rate of a protein fibril (Calvez et al., 2009). Modelers usually assume that fibrils below a critical size have a negligible tendency to grow, because of instability of small aggregates (Garzón et al., 2021; Masel et al., 1999; Prüss et al., 2006). This is in line with experimental evidence that shows that very short fibrils have nil converting activity (Silveira et al., 2005; Kim et al., 2012). There is also some evidence that very short fibrils are unstable, which would explain their very low converting activity (Pieri, Madiona, & Melki, 2016). Hence, whenever a protein fibril below a critical size arises (due to breakage), it is assumed that it immediately degrades into non-infectious monomers that can again be incorporated into fibrils (Garzón et al., 2021; Greer et al., 2006; Masel et al., 1999). Fibrils above a critical size are thought to be more stable and can therefore elongate further. From practical studies it turns out that there is a non-linear relationship between the propensity of a prion fibril to propagate and its length above critical size. By way of example, it was found that both very short and lengthy fibrils had a relatively low converting activity. On the contrary, a peak in the converting activity was seen for fibrils of short length (Silveira et al., 2005). It is also known that agitation of an infectious protein solution can cause fibrils to break and shorten (Sakunthala et al., 2022; Tarutani et al., 2016; Weber et al., 2007; Weber, Reznicek, Mitteregger, Kretzschmar, & Giese, 2008). And indeed, when prion fibrils are exposed to agitation, their propensity to propagate increases, as is indicated by increased seeding efficacy (Tanaka, Collins, Toyama, & Weissman, 2006). This implies that short fibrils have a higher tendency to elongate than longer fibrils. Very recently, some researchers found that the length of fibril seeds correlated strongly and negatively with their elongation rate (k_+)

($R^2 = 0.99$) (Sakunthala et al., 2022). This relationship between fibril length and elongation rate seems robust. A similar relationship was found in two studies of a decade earlier for a different protein strain (Xue, Hellewell et al., 2009; Xue, Hellewell, Hewitt, & Radford, 2010). However, authors claim that this inverse relationship is not due to an intrinsic property of short fibrils to elongate faster. Also, they seemingly did not measure the elongation rate per fibril (per capita growth rate), but the total elongation rate. In their experimental procedure they added a sample of sonicated fibrils to a new solution of monomers each time. It is more likely that short fibrils in such a sample are more outnumbered than longer fibrils. This leads to a situation with more elongation-potent fibril ends. As the authors of these studies state, it is this mechanism that explains the higher elongation rate of shorter fibrils (Sakunthala et al., 2022; Xue, Hellewell et al., 2009). Rather, researchers find a simple linear relationship between the length of individual fibrils and the elapsed time. This indicates that the rate of elongation is constant (Eves et al., 2021; Goldsbury, Kistler, Aebi, Arvinte, & Cooper, 1999; Qiang, Kelley, & Tycko, 2013; Zimmermann et al., 2021). In this work, we thus assume that the intrinsic elongation rate of protein fibrils is constant.

Model assumption 4

For the degradation rate, it was mostly assumed that it remains constant, irrespective of polymer size (Engler et al., 2006; Garzón et al., 2021; Greer et al., 2006, 2007; Masel et al., 1999; Prüss et al., 2006; Rubenstein et al., 2007). In just few cases, the degradation rate was considered to be dependent on the length of the prion polymer (Prigent et al., 2012). Indeed, experimental studies show that resistance to degradation varies with size of the prion polymer (Igel-Egalon et al., 2020; Laferrière et al., 2013; Tixador et al., 2010; Tzaban et al., 2002). However, making the degradation rate length dependent is difficult, as the degradation rate as a function of length is not well known. Thus, like most other studies, we keep the degradation rate of polymers constant.

Model assumption 5

Next, there is the joining of fibrils, which can happen with an end-to-end mechanism, as discussed in (Greer et al., 2007) or with lateral association. There is some mechanical evidence for the end-to-end mechanism, but this should be treated with caution as it was only seen in a synthetic, non-biological protein strain (Arosio, Owczarz et al., 2012). There seems to be mixed evidence for the lateral association of fibrils. Some researchers clearly suggest that fibrils can associate laterally with each other (Ionescu-Zanetti et al., 1999; Khurana et al., 2003). Others observe this lateral association only carefully within specific solution conditions (Nichols et al., 2002) and argue that elongation of fibrils by monomer addition is predominant (Qiang et al., 2013). To simplify this complex issue, we assume in this article that lateral association of fibrils is a negligible process.

Treatment options

Next to the assumptions that we take into account, there is also another important aspect that was not added in most models, but should be added in the model of this study. This aspect is the presence of treatment options. This aspect is essential, because in this study, we need to assess how breakage parameters mediate treatment effects. For example, Garzón et al. (2021) theoretically assessed methods of treatment in their model. More precisely, they assessed the influence of combined treatment of chaperones and interferons on prion dynamics. In addition to the (negligible) natural degradation rate of prions, interferons add an extra degradation term to the normal degradation rate

in the model. This idea is based on insights from molecular studies that show that interferons impede the propagation of prions by facilitating their degradation. Chaperones suppress prion aggregation as well [e.g. (Allen et al., 2005; Jin et al., 2000; Park et al., 2017; Son & Wickner, 2020)]. They can do this by refolding improperly folded protein monomers (Wu, Stull, Lee, & Bardwell, 2019). This can be modeled by adding an equation for the chaperone population and the interaction between chaperones and prion monomers. They found that the theoretical administration of either treatment was enough to lower the reproductive ratio, such that the proliferation of prions could be curbed. It could be observed that the maximal prion concentration reduced as the dose of interferons increased. A combined treatment even led to a complete theoretical abolishment of misfolded prion proteins (Garzón et al., 2021). However, a critical notion to how Garzón et al. (2021) modelled the role of chaperones should be made. They assumed that chaperones bind to healthy monomers and would therefore protect these monomers from misfolding. However, empirical and simulation studies show that chaperones not only bind to healthy proteins in native state (Petrosyan, Patra, Rezajooei, Garen, & Woodside, 2021) but to misfolded proteins as well and refold them to a healthy state again (Wyszokowski et al., 2021; Lu et al., 2021). Therefore, in addition to that of Garzón et al. (2021), we include an association interaction between misfolded monomers and chaperones as well.

The current study

Global study design

The current study tries to combine previous modeling techniques to assess the influence of (combined) treatment of chaperones and interferons on prion proliferation dynamics. In contrast to other studies, this study relaxes on 2 of the 3 basic assumptions mentioned in the literature review in the introduction. The combination of influence of different treatments and the modification of two of the three basic assumptions makes this study unique.

We introduce the adaptations in a step-wise manner. Doing this, we first reproduce basic prion dynamics for every combination of treatment and assumptions, including a logistic decay and growth curve over time of monomers and polymers, respectively. We show the (biphasic) dynamics of the mean prion fiber length over time and reproduce a probability density function of the prion fiber length without treatment and with combined treatment with chaperones and interferons. Secondly, we investigate the relationship between the reproductive ratio and increasing treatment doses in the same manner. Thirdly, and most important, we show how sensitive the prion propagation dynamics are to changes in the position and length dependence of prion breakage. This has important implications, as it tells us if neglecting such dependencies influences our estimates of prion propagation. Below, we define the assumptions of the literature-based combined model. In addition, we restate the methods of treatment:

1) **The breakage rate is non-linearly dependent on the length of the protein fibril and follows a power law;**
2) **The likelihood of breakage is dependent on and follows a parabolic relationship with the position of breakage;**
3) The elongation rate above a critical fibril size is constant and fibrils only elongate by monomer addition

Then, the methods of treatment are:

a) A dosage of chaperones
b) A dosage of interferons

In the next section, the current model is explained in detail.

The prion breakage-elongation dynamic model

Model scheme and parameter definitions

Respecting the discussed literature, see the following schematic of the proposed model (**Figure 2**). The gross design of the model is based on Garzón et al. (2021). However, some important changes are proposed. For example, we include different length classes for the polymers in our model. Next, we have a non-constant breakage rate kernel $\kappa(i,j)$ and per-capita elongation rate ε. Here, i is the length of the protein fibril and j is the position of the fibril. In short, $\kappa(i,j)$ is a measure for the probability of a fibril of length i to break at position j. Hence, the breakage rate may depend upon the length i of the prion fibril and the position of the breakage j in the prion fibril (Beal et al., 2020; Nicoud et al., 2015).

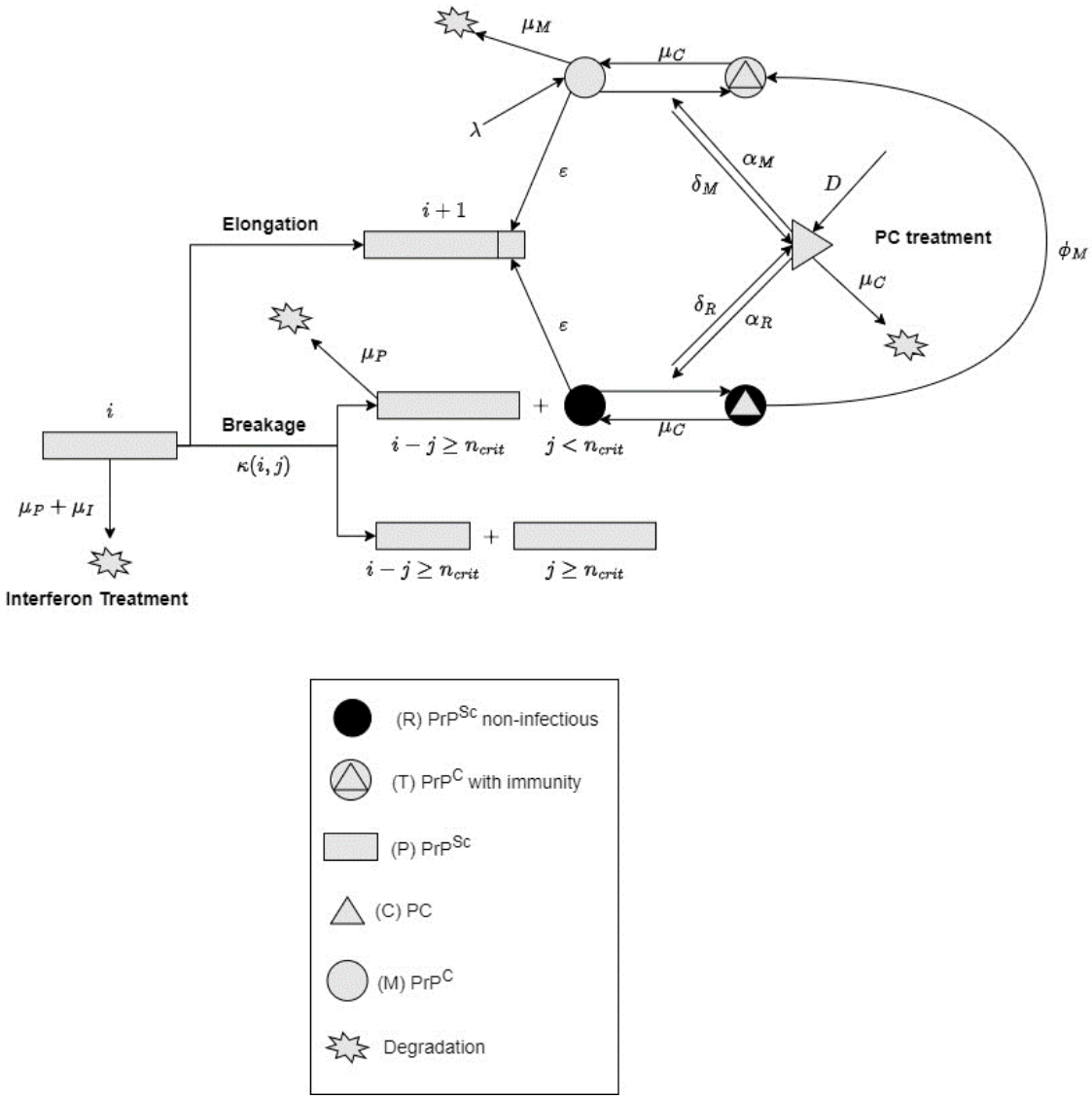

Figure 2. The proposed prion aggregation population. See the following sections for an in-depth description of the different processes, and differences between the current model and its predecessor developed by Garzón et al. (2021).

Table 1. Table of parameters and their description.

Name	Description
State variables	
S	Susceptible population of PrP^{C}
T	PrP^{C} proteins treated with pharmacological chaperones
P	PrP^{Sc} chains
L	Mean length of PrP^{Sc} polymers
O	Oligomers smaller than x_0
C	Pharmacological chaperone population

Parameters

λ	Natural production of PrP^C
μ_S	Degradation rate of PrP^C
μ_P	Degradation rate of PrP^{Sc} polymers
μ_R	Degradation rate of PrP^{Sc} monomers
μ_C	Degradation rate of pharmacoperones
μ_I	Degradation rate of PrP^{Sc} due to interferons
α	Binding rate of pharmacoperone to PrP^{Sc}
x_0	Minimum polymer length
D	Daily dosage of pharmacological chaperones
k_E	Elongation rate constant
k_{B_1}	Breakage rate constant
k_{B_2}	Breakage rate-length power
k_{B_3}	Breakage position preference constant

Functions, chemical reactions and model definition

In this paragraph, important functions are defined. The previously discussed parameters serve as building blocks to derive the model. All of the dynamics in the model are based on mass-action kinetics. First, we discuss the dynamics of the monomers and their binding with chaperones. Next, the formation of fibers is discussed. Finally, the process of fiber breakage is explained. Several rates of processes are described, together with relevant chemical reactions.

Model dynamics of the monomers

Below, we define and explain the processes that are related to healthy and misfolded monomers. Healthy monomers are produced with a rate λ. Healthy monomers and misfolded monomers decay with a rate that is proportional to their concentration, $\mu_M M$ and μ_R, respectively. Here, μ_M and μ_R are rate constants. M and R represent the concentration of healthy and misfolded monomers, respectively.

Interactions between monomers and chaperones

Monomers interact with chaperones as well. firstly, there is association of monomers with chaperones. This happens at rate $\alpha_M CM$ and $\alpha_R CR$ for healthy and misfolded chaperones, respectively. α_M and α_R are association rate constants for healthy and misfolded monomers,

respectively [rightward arrows of reactions (Ia) and (Ib)]. Here, C represents the concentration of the chaperones that are administered at rate D. Next to this, there is also the dissociation of a healthy and misfolded monomer from a monomer-chaperone complex. This is represented by $\delta_M T_M$ and $\delta_R T_R$, respectively. Here, δ_M and δ_R represent the rate constants for the healthy monomers respectively [leftward arrows of reactions (Ia) and (Ib)]. Lastly, there is the correct folding rate of misfolded monomers into correctly folded (healthy) monomers, $\phi_M T_R$. ϕ_M is the correct folding rate constant [see also reaction (II)].

$$M + C \rightleftharpoons CM \quad (\mathrm{Ia})$$

$$R + C \rightleftharpoons CR \quad (\mathrm{Ib})$$

$$CR \rightarrow C + M \quad (\mathrm{II})$$

Polymer kinetics

Next, there are the polymer kinetics. Firstly, polymers of length i can elongate with one (misfolded) monomer, to form a polymer of length $i + 1$. This happens at rate $\varepsilon M P_i$ and $\varepsilon R P_i$ for healthy and misfolded monomers, respectively [see reactions (IIIa) and (IIIb)]. Fibers have a minimal length of n and a maximal length of N. Furthermore, fibers can decay at a rate $(\mu_P + \mu_I)P_i$. Here, μ_P is the natural degradation rate constant and μ_I is the degradation rate constant due to interferons. In the next paragraph, the polymer breakage kinetics are discussed.

$$P_i + M \rightarrow P_{i+1} \quad (\mathrm{IIIa}), \quad n \leq i \leq N$$

$$P_i + R \rightarrow P_{i+1} \quad (\mathrm{IIIb}), \quad n \leq i \leq N$$

Fibril breakage rate and position functions

First, there is the discrete breakage rate function $\beta(i)$, which is defined as

$$\beta(i) = \beta_1 i^{\beta_2} \quad (2);$$

Where β_1 is the primary breakage rate constant and β_2 is the power of the relationship between length and rate (Nicoud et al., 2015) If $\beta_2 < 0$, this would mean that shorter fibers are absolutely more likely to break than longer fibers. We do not believe that this is likely because of well-known force-moment relationships. Now, there is another function $\Gamma(i, j)$ that represents the daughter distribution. This distribution describes the probability of an i-sized fibril to break at a given position j, with respect to all other possible breakage events that an i-sized fibril may undergo (Nicoud et al., 2015). Nicoud and others (2015) derived an easy-to-use kernel to describe the daughter distribution. Here, we used a discretized version of their kernel:

$$\Gamma(i, j) = \frac{1 + k_{\beta_3}\left(\frac{2j - i}{i}\right)^2}{\sum_{k=1}^{i-1}\left(1 + k_{\beta_3}\left(\frac{2k - i}{i}\right)^2\right)} \quad (3)$$

Paying attention to the constant β_3, we can distinguish the following three cases. If $\beta_3 > 0$, then the erosion mechanism is in effect, i.e. fibers have a tendency to break at one of the ends. If $\beta_3 < 0$, then we get a center mechanism and the fiber is more likely to break in the middle. Lastly, if $\beta_3 = 0$, the fiber can break at any position with equal likelihood. The daughter distribution kernel and breakage rate together make up the entire breakage kernel $\kappa(i,j)$, which is defined as in (Nicoud et al., 2015), but is discrete here:

$$\kappa(i,j) = \beta(i)\Gamma(i,j) \quad (4)$$

This breakage kernel is important, as it essentially describes the time evolution of the average fibril length for any protein fibril type (Nicoud et al., 2015; Xue & Radford, 2013). μ_P is the polymer degradation constant. Below the minimal size n, we assume that polymers become unstable and fall apart (Pieri et al., 2016).

Now that we have defined the breakage kernels, we can assign breakage rates to several polymer breakage processes. For example, there is the breakage of fibrils of length i into smaller fibrils. This happens at rate $P_i \sum_{j=1}^{i-1} \kappa(i,j)$, since there are $i-1$ possible positions at which a fiber can break. Besides, larger fibers of length j can break into two fibers, either of which has length i. This happens at rate $P_j \sum_{j=i+1}^{N} \big(\kappa(j,i) + \kappa(j,j-i)\big)$.

$$P_j \to P_i + P_{j-i} \quad \text{(IVa)}, \qquad i, j-i \geq n$$

$$P_j \to iR + P_{j-i} \quad \text{(IVb)}, \qquad i < n \wedge j - i \geq n$$

$$P_j \to (j-i)R + P_i \quad \text{(IVc)}, \qquad i \geq n \wedge j - i < n$$

$$P_j \to jR \quad \text{(IVd)}, \qquad i, j-i < n$$

The total ordinary differential equation model

Below, the resulting total model is the following. Of special note are the terms $\varepsilon M \sum_{i=n}^{N-1} P_i$ and $\varepsilon R \sum_{i=n}^{N-1} P_i$ that denote the incorporation of monomers into fibrils of all length classes. Furthermore, there is no inflow of polymers of the smallest length due to elongation, because polymers smaller than n fall apart. In the same way, there is no inflow of polymers of the largest length N due to breakage of larger polymers. Also, there is no outflow of the largest polymers due to elongation into even larger polymers.

$$\frac{dM}{dt} = \lambda + (\delta_M + \mu_C)T_M - \left(\alpha_M C + \mu_M + \varepsilon \sum_{i=n}^{N-1} P_i\right) M \quad (5a)$$

$$\frac{dP_i}{dt} = -P_i\left(\mu_P + \mu_I + \sum_{j=1}^{i-1}\kappa(i,j)\right) + \begin{cases} -\varepsilon(M+R)P_n + \sum_{j=n+1}^{N}\big(\kappa(j,n)+\kappa(j,j-n)\big)P_j\,, & \text{if} \quad i=n \quad (5b) \\ \varepsilon(M+R)(P_{i-1}-P_i) + \sum_{j=i+1}^{N}\big(\kappa(j,i)+\kappa(j,j-i)\big)P_j\,, & \text{if } n<i<N \quad (5c) \\ \varepsilon(M+R)P_{N-1}\,, & \text{if } i=N \quad (5d) \end{cases}$$

$$\frac{dR}{dt} = -\left(\mu_R + \alpha_R C + \varepsilon\sum_{i=n}^{N-1}P_i\right)R + (\delta_R+\mu_C)T_R + \sum_{j=1}^{n-1}\sum_{i=n}^{N} j\big(\kappa(i,j)+\kappa(i,i-j)\big)P_i \quad (5e)$$

$$\frac{dT_M}{dt} = \alpha_M CM - (\delta_M+\mu_C+\mu_M)T_M + \phi_M T_R \quad (5f)$$

$$\frac{dT_R}{dt} = \alpha_R CR - (\delta_R+\mu_R+\mu_C+\phi_M)T_R \quad (5g)$$

$$\frac{dC}{dt} = D - (\alpha_M M + \alpha_R R + \mu_C)C + (\delta_R+\mu_R)T_R + (\delta_M+\mu_M)T_M \quad (5h)$$

Data analysis and model read-outs

The state variables are the primary model read-outs. These are collected for each timepoint during the simulation. The state variables include the healthy (M) and misfolded monomer concentration (R), all of the polymer concentrations of length i, with $n \leq i \leq N$ (P_i), the chaperone-bound healthy (T_M) and misfolded monomer concentration (T_R), and finally, the chaperone concentration (C). Next to these primary read-outs, there are special primary read-outs and exogenous variables.

The reproductive ratio is an a special case of a read-out variable and is calculated as follows. First, a healthy equilibrium was created by setting the initial conditions such that only monomers were in the solution. Next, this healthy equilibrium was then used to initiate a next simulation session. During the first timestep of this simulation, a small amount of polymers was added to the solution. Next, the model was run in a loop and values were updated. For each timestep we calculated the normalization factor as the quotient between the initialized concentration of polymers and the density of all the fibers for each time step. Then, the negative logarithm of R_0 was calculated by taking the logarithm of the normalization factor divided by the length of the interval between two timesteps. Then R_0 is calculated by exponentiating the former. The entire formula for R_0 is written down below

$$R_0 = e^{\frac{\ln\left(\frac{R(t)+T_R(t)+\sum_{i=n}^{N} iP_i(t)}{[P]_{init}}\right)}{\Delta t}} \Leftrightarrow$$

$$R_0 = \left(\frac{R(t)+T_R(t)+\sum_{i=n}^{N} iP_i(t)}{[P]_{init}}\right)^{\frac{1}{\Delta t}} \quad (6)$$

On the other hand, exogenous variables of the model are variables that are calculated after the simulation is finished. Here, exogenous variables include: total protein fibril concentration; $[P_{Total}]$, total protein fibril mass; Z_P, total infected mass; Z_{Inf}, total biological mass; Z_{Total}, mean length; $\bar{L}$ and mean breakage rate $\bar{\kappa}$. The definitions of these variables are listed below:

$$[P_{Total}(t)] = \sum_{i=n}^{N} P_i(t) \quad (7)$$

$$Z_P(t) = \sum_{i=n}^{N} iP_i(t) \quad (8)$$

$$Z_{Inf}(t) = R(t) + T_R(t) + \sum_{i=n}^{N} iP_i(t) \quad (9)$$

$$Z_{Total}(t) = M(t) + R(t) + T_M(t) + T_R(t) + \sum_{i=n}^{N} iP_i(t) \quad (10)$$

$$\bar{L}(t) = \frac{\sum_{i=n}^{N} iP_i(t)}{\sum_{i=n}^{N} P_i(t)} \quad (11)$$

$$\bar{\kappa}(t) = \frac{\sum_{i=n}^{N} P_i \sum_{j=1}^{i-1} \kappa(i,j)}{\sum_{i=n}^{N} iP_i} \quad (12)$$

Now that we have clarified the design of the study together with the prion fibril aggregation model, we can show the experimental design.

Experimental design

The following experimental design is shaped towards the research questions we want to address. The experimental design is partitioned into three parts: model validation, univariate analysis, and bivariate or mediation analysis.

Model validation

The model validation part is simply meant to test whether the state variables follow the dynamics as seen in previous studies. As indicated in **Figure 1**, the blue rectangle with the key parameters β_2, β_3, μ_I and D. Here, all state variables (and exogeneous variables as well) are plotted against time. Furthermore, the evolution of the length distribution is plotted in a color plot, where distributions are taken over time. Here, color represents time. biologically seen, the above means that we assess the basic dynamics of the model without any treatment. Furthermore, the breakage rate is set as linearly dependent on length of the protein fibril. Also, the likelihood of breakage is assumed equal across all fibril sites.

In the second part, one of the four key parameters is varied each time: the chaperone dosage (D), interferon dosage (μ_I), length-dependent breakage (β_2) or the position-dependent breakage parameter (β_3). Again, the state variables are plotted against time, grouped by one of the four key parameters. The same is done for the *stable* length distribution; only one time point, but grouped by a key parameter. If necessary, the regular plots are clarified with help of contour plots. In **Figure 1**, the second part is called **Univariate analysis**.

In the third and last part, we do a **Bivariate analysis** or mediation analysis. In this part, we look at how the breakage parameters mediate the treatment effects on prion propagation. We do this by plotting each state variables against different values for treatment parameters, grouped by breakage parameter in a regular plot. Here again, contour plots are used if necessary. Unique to this part is that we can perform an analysis on the critical value of the reproductive ratio R_0. To clarify, the critical value of R_0 is 1. The minimal treatment dose for which $R_0 < 1$ is called the critical dose. The question here is: How do the breakage parameters influence the critical dose? In the next paragraph, the hypotheses are stated in more detail. In the next section, a prion breakage-elongation model is proposed, based on the reviewed literature.

In all of the experimental settings, the default parameter values (not key parameter) were set at $n = 4; \lambda = 2; \alpha_M = 0.02; \alpha_R = 0.4; \delta_M = 0.4; \delta_R = 0.02; \phi_M = 0.4; \mu_C = 0.001; \mu_M = 0.05; \mu_R = 0.05; \mu_P = 0.005; \varepsilon = 0.16; \beta_1 = 0.04; \beta_2 = 1; \quad \beta_3 = 0$. Initial conditions were $M(0) = 500$, $P_{n\to 4}(0) = 0.001$ and all other initial values were set at 0. In case R_0 was calculated, the initial healthy equilibrium conditions were $M(0) = \frac{\lambda}{\mu_M}$, $C(0) = \frac{D}{\mu_C}$.

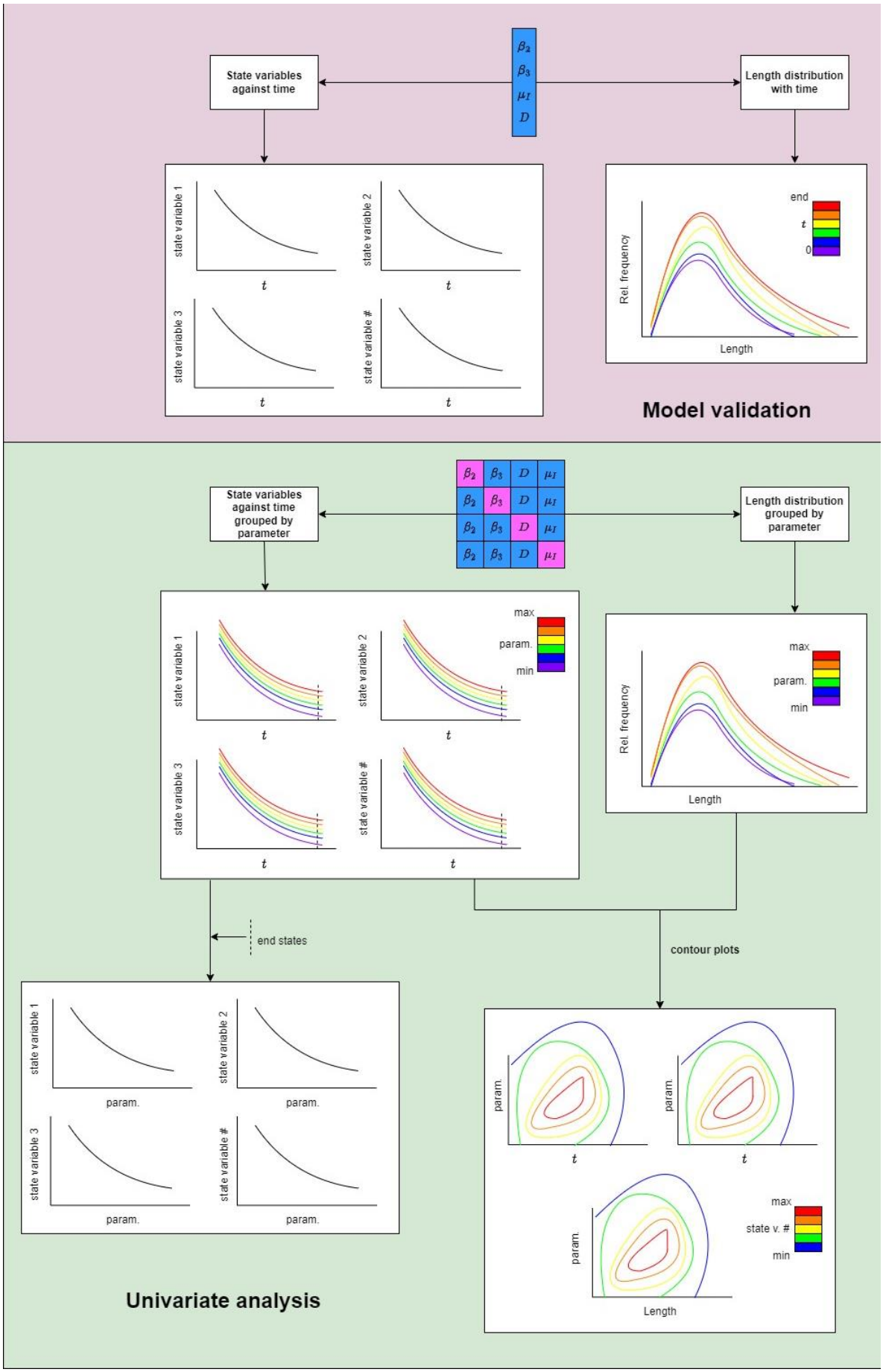
State variables against time
β_2
β_3
μ_I
D
Length distribution with time
state variable 1
state variable 2
state variable 3
state variable #
t
Rel. frequency
Length
end
t
0
Model validation
State variables against time grouped by parameter
Length distribution grouped by parameter
max
param.
min
end states
contour plots
param.
state v. #
Univariate analysis

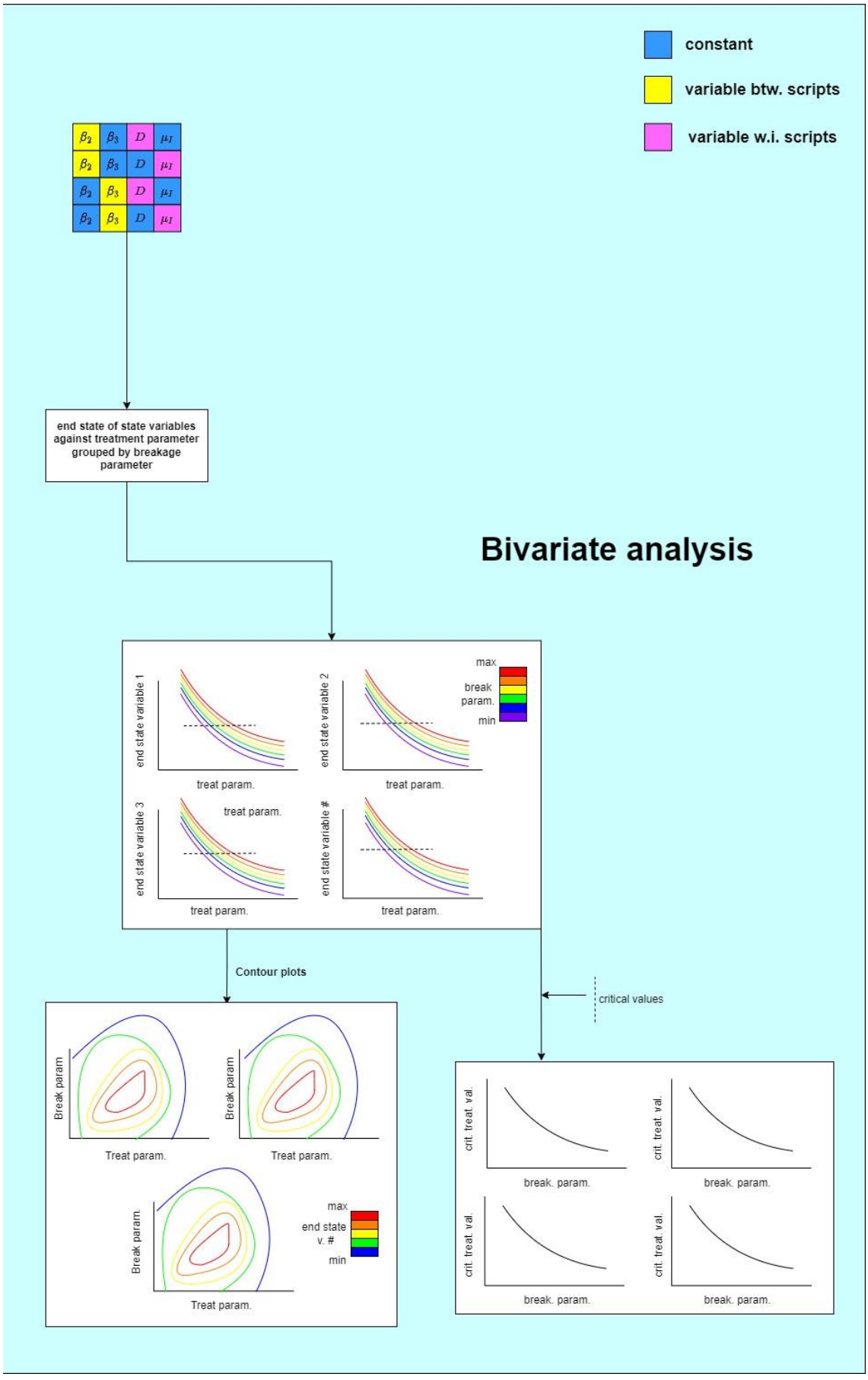
constant
variable btw. scripts
variable w.i. scripts
β_2 β_3 D μ_I
β_2 β_3 D μ_I
β_2 β_3 D μ_I
β_2 β_3 D μ_I
end state of state variables against treatment parameter grouped by breakage parameter
Bivariate analysis
end state variable 1
treat param.
end state variable 2
treat param.
max
break param.
min
end state variable 3
treat param.
end state variable #
treat param.
Contour plots
critical values
Break param
Treat param.
Break param
Treat param.
Break param.
Treat param.
max
end state v. #
min
crit. treat. val.
break. param.
crit. treat. val.
break. param.
crit. treat. val.
break. param.
crit. treat. val.
break. param.

(continued)

Figure 1. Experimental design and expected results.

Results

Part I – model validation

Chaperones and interferons potentially reduce prion polymer mass

The first results show that chaperones and interferons in this model reduce the prion polymer mass. The highest polymer mass concentration was reached when there was no treatment. Interferons qualitatively reached the same effect, but a bit stronger. Combined treatment led to a (nearly) complete abolishment of polymers, according to the model (**Figure 1**). The critical polymer size was set at 4 and the upper bound for polymer size was set at 50. Furthermore, it could logically be seen that the number of bound (infected) monomers was increased when chaperones were introduced. Remarkably, the concentration of bound monomers became lower when interferons were added. An explanation for this is that interferons directly degrade polymers by an extra degradation term. As a consequence, there are fewer polymers that can shed off misfolded monomers (**Figure S1C**). This can lead to a situation in which fewer misfolded monomers are bound by chaperones (**Figure S1A**).

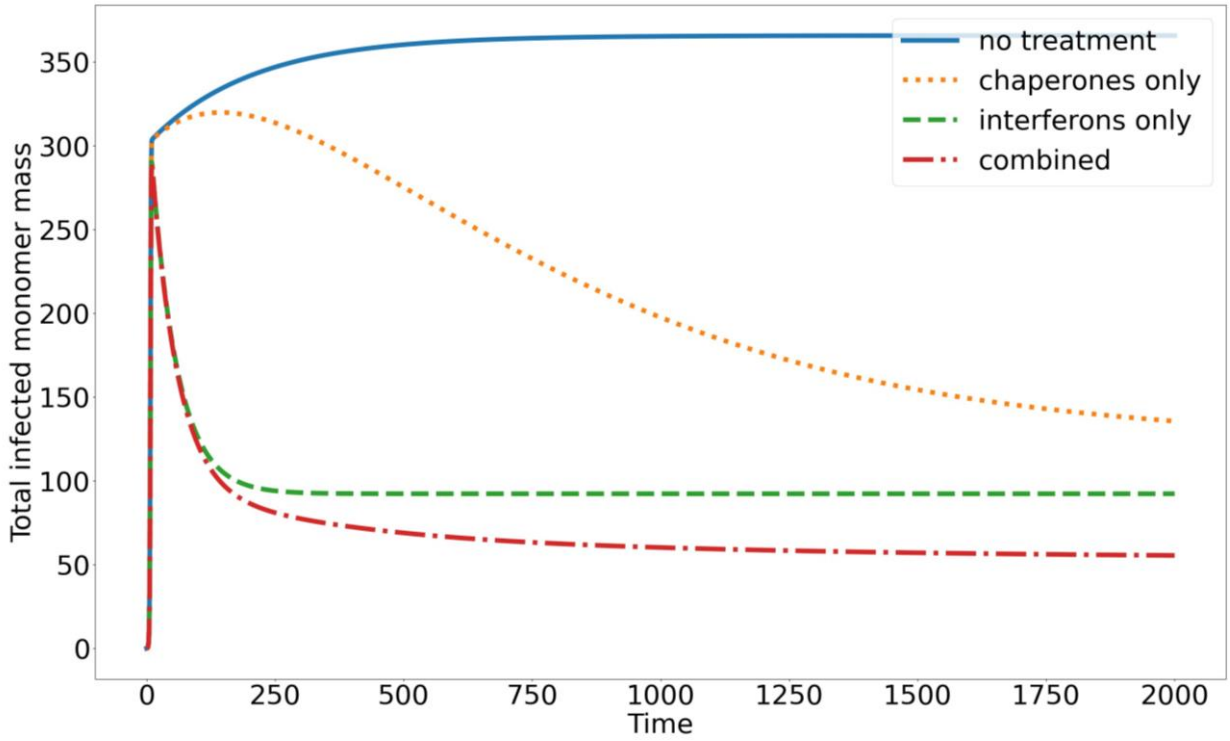

Figure 1. Total infected monomer mass concentration plotted against time for four treatment regimes. Blue line: no treatment; yellow line: only chaperones; green line: only interferons; red line: combined treatment. Relevant parameter settings are, in respective order: $(D, \mu_I) = \{(0,0), (0.040,0), (0,0.015), (0.040,0.015)\}$.

Healthy monomers decay under pathological conditions

With pathological conditions, it is meant that a tiny amount of linear protein aggregates is present. We expected that normal protein monomers decrease in abundance according to partial logistic decay curve. This is partial because the nucleation step is not incorporated into the model. Hence, the lag phase of monomer depletion will vanish. Thus, as expected, healthy monomers decay under pathological conditions. This happens with a near-sigmoidal curve. An explanation for the steep drop at already the beginning of time could be that we immediately provide the system with a tiny amount of these linear aggregates. This provision step circumvents the more slow formation of a nucleus (**Figure 2**).

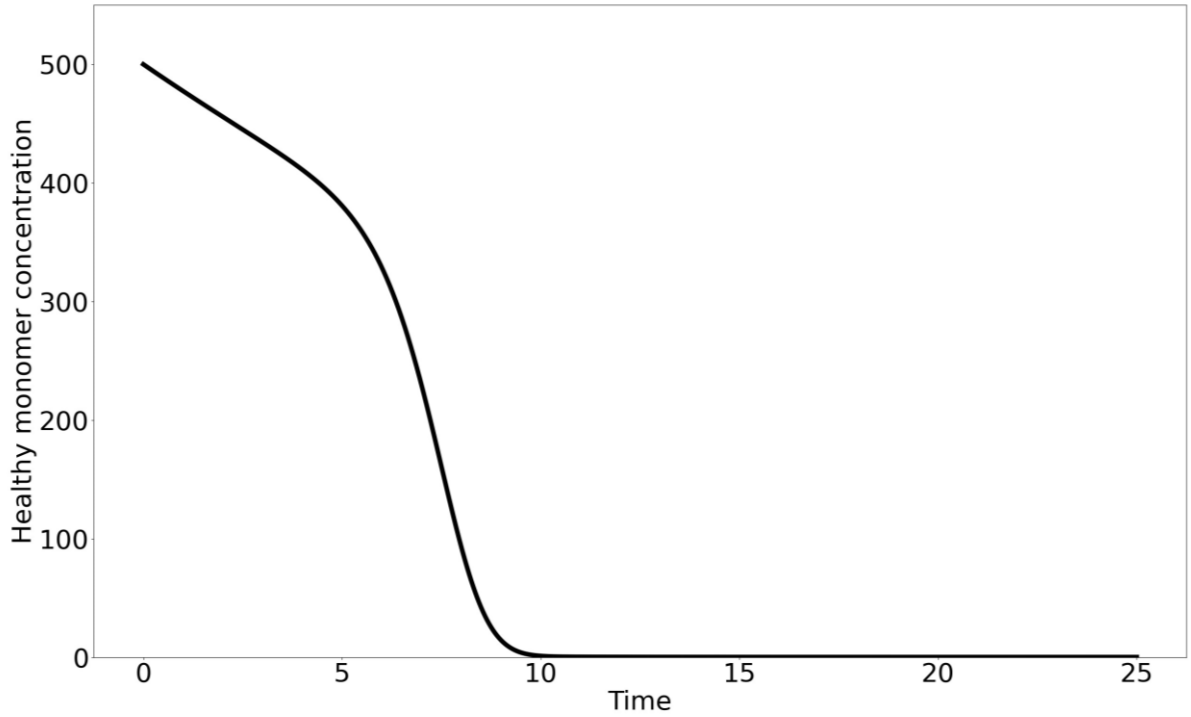

Figure 2. Plot of healthy monomer concentration against time.

Infective polymer mass increases under pathological conditions

it was expected that prion fibers proliferate according to a logistic growth curve. However, infected protein monomers will slowly increase according to a full logistic growth curve. This is because the formation of polymers is required first. After that, polymers were expected to break into smaller pieces and eventual infected monomers. This indicated that there would be a lag phase in the formation of infected monomers. The polymer concentration and polymer mass would increase logistically, without a lag phase as the simulation is already initialized with some protein fibers.

And, roughly as expected, the infective polymer mass increases under pathological conditions. Firstly, there is a short lasting lag phase. This was not expected, because a bit of protein aggregates was thrown in the solution already at the beginning of the simulation. An explanation for this, is the low initial value of 0.001 of just the smallest polymer length class n. Greater initial concentrations indeed cause an abolishment of the lag phase (see **Supplementary figure 2A** and **B**). After that, there is exponential growth. Stagnation of the total polymer mass occurs in the last phase, due to monomer depletion as seen in **Figure 2** (**Figure 3A, B**). For the free infected monomer concentration, there was indeed a lag phase (**Supplementary figure 3**).

A **B**

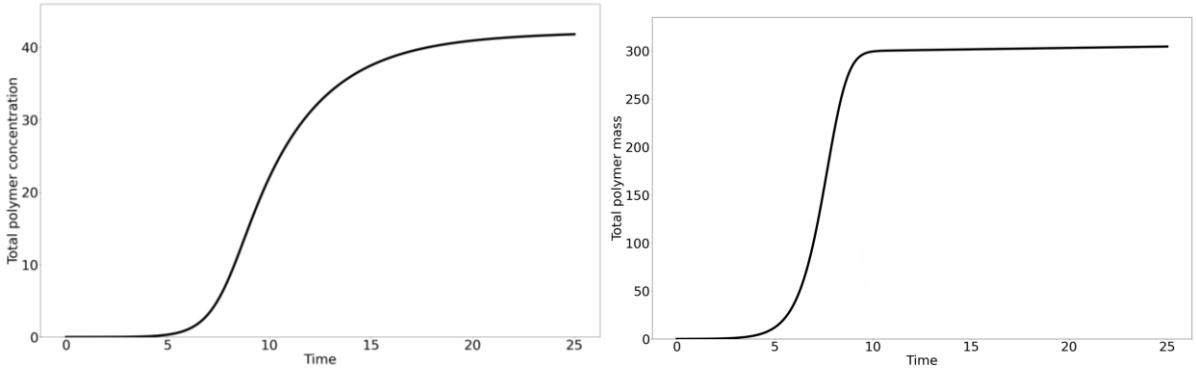

Figure 3. Plot of total polymer concentration **A)** and mass **B)** against time.

Linear protein aggregates fragment over time

For the mean length of prion fibers, it was hypothesized that it changes in a biphasic manner over time. First, the mean length would increase. Then the mean length would decrease and reach equilibrium. This mean length is also the mean of a right-skewed probability density of the length of prion fibers in general. And, as can be seen from **Figure 4**, it became clear that linear protein aggregates fragmented as time passed. Firstly, there was the phase of rapid elongation of tiny amounts of short aggregates to longer aggregates. Here, elongation of polymers was dominant (**Figure 4A**). In **Figure 4B** and **Figure 4C**, it can be seen that there were relatively more fibers of greater length. After a while, we see that the mean aggregate (polymer) length drops (**Figure 4A**). During this phase, breakage is dominant, as can be seen by a shift towards shorter polymer lengths in the length distribution over time (**Figure 4B**, **C**). After this, the mean aggregate length tends towards an equilibrium. This can be seen from a flattening line (**Figure 4A**) and a stabilizing length distribution (**Figure 4B**, **C**).

A **B**

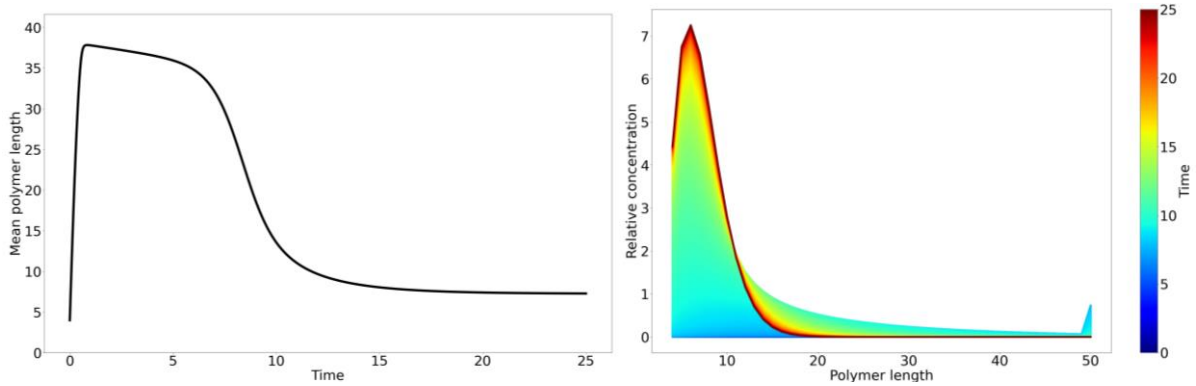

C

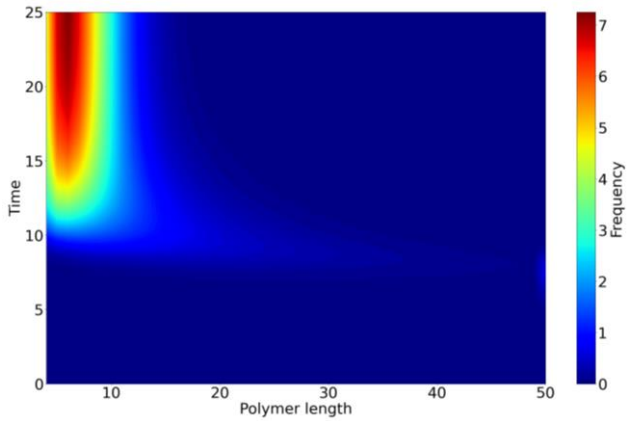

Figure 4. A) mean linear protein aggregate length (in monomers) plotted against time. **B)** Color plot of the length distribution of linear protein aggregates with the coloring dependent on the point in time. **C)** Filled contour plot of the length distribution seen from above over time.

Part II – univariate analysis

An increasing length-dependent breakage fastens the formation of infected protein mass and determines infectivity in a non-linear way

The length dependence in the breakage rate tells us how likely it is that long fibers break relative to short fibers. A $\beta_2 > 1$ tells that long fibers are relatively more likely to break than shorter fibers. In the case that $0 < \beta_2 < 1$, shorter fibers are relatively more likely to break than longer fibers. The following 30 equally spaced values for β_2 were chosen

$$\mathbf{B_2} = [0, \dots, 2.9]$$

In this experiment, we had the following expectations. The power in the length-dependent breakage influences the mean length of the arising prion fibers. A stronger-than-linear power law makes that longer fibers are relatively more likely to break than shorter fibers. This results in a smaller mean length and a more right-skewed distribution of fiber length. A weaker-than-linear relationship brings about a situation in which long fibers are relatively less likely to break. This will result in a larger mean length and a less pronounced right skewness. However, it is assumed that long fibers are *absolutely* more likely to break than short fibers. And as expected, a stronger power in the length-dependence accelerates the fragmentation and thus the propagation of linear protein aggregates. This can be inferred from the fact that the mean aggregate length is lower for a higher β_2 at the same time point (**Figure 5A, B**). For higher values of β_2, there was also a more pronounced right-skewed length distribution (**Supplementary figure 4**).

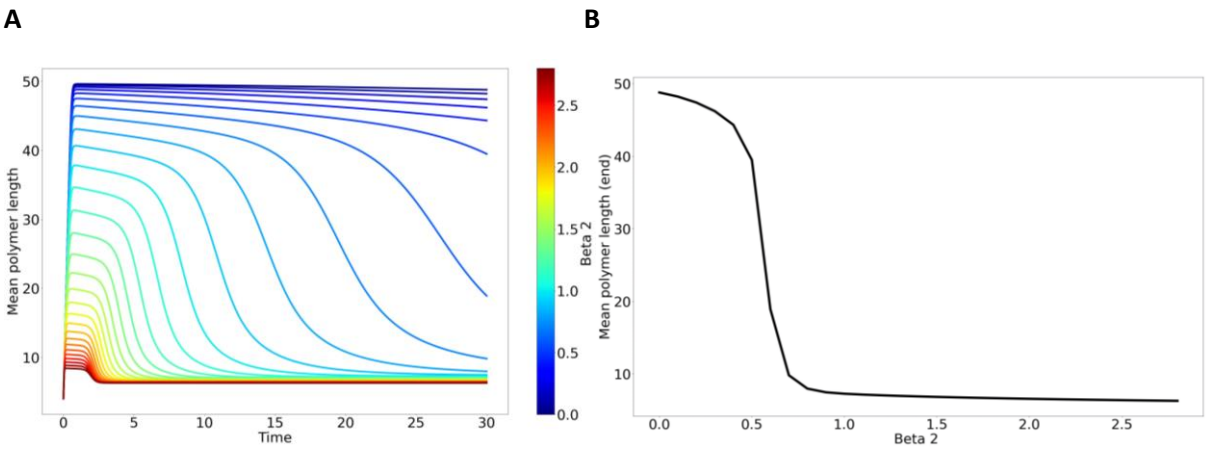

Figure 5. A) The mean polymer length plotted against time grouped by values for β_2 and **B)** end-simulation value of the mean length plotted against values for β_2 (power of length-dependence).

Also, according to this model, the infectivity of a protein aggregate solution is especially determined by the amount of linear protein aggregates equal to or greater than the minimal nucleus size. This is because only the linear aggregates are able to elongate. Having said this, we see that there is a global increase in the total polymer mass at first sight (**Figure 6A**). However, when we look at the end-simulation polymer mass, there is a non-linear relationship with β_2. First, the polymer mass increases, reaches a maximum and then decreases (**Figure 6B**). A possible explanation for this is that weak to moderate length-dependence enhances the fragility of long aggregates and thus breakage of long aggregates. This contributes to the propagate of linear aggregates. However, when the length-dependence becomes too strong, fibers in general become more fragile and are likely to fall apart into infected monomers anyhow. The latter is supported by the fact that the end-simulation concentration of free infected monomers rises as aggregates become more fragile (i.e. have a higher β_2) (**Figure 6C, D**). Thus, a moderate length-dependence stimulates the propagate of linear aggregates. On the contrary, a very strong length-dependence hampers the propagate of linear aggregates as they are too likely to fall apart in non-infectious monomers. In the same way, this *optimality* phenomenon of the length-dependence has its backlash on the reproductive ratio (**Figure 6E**).

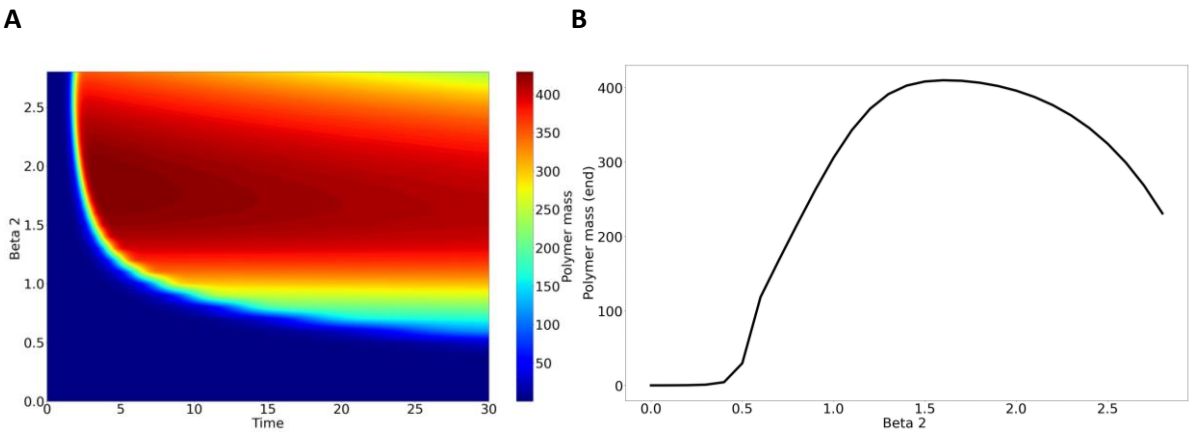

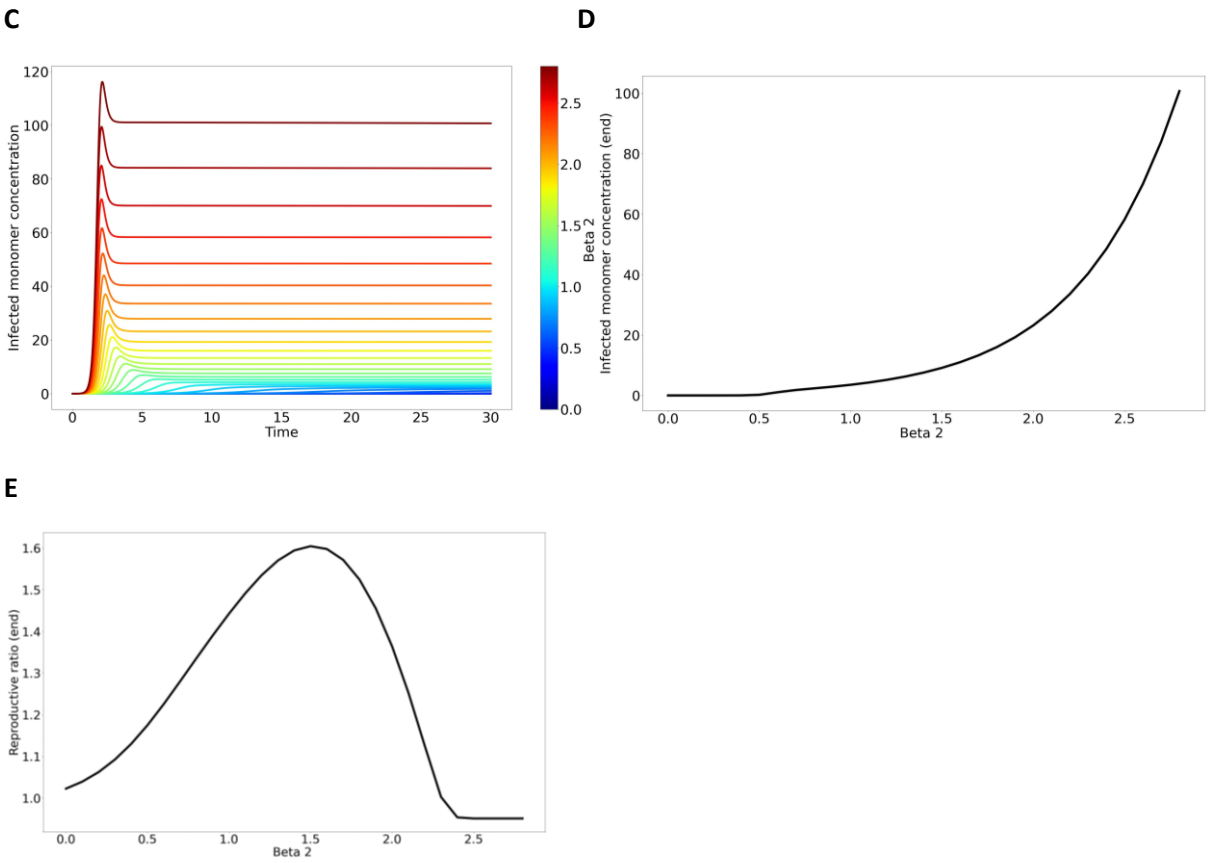

Figure 6. A) contour plot of the total polymer mass over time (horizontally) and values of β_2 (power of length-dependence), **B)** end-simulation polymer mass plotted against β_2, **C)** color plot of infected free monomer concentration against time grouped by β_2, **D)** end-simulation concentration of infected free monomers plotted against β_2, and **E)** end-simulation reproductive ratio against β_2.

A center-breakage mechanism favors the propagation and sustention of (shorter) linear protein aggregates

To remind the reader, center-breakage is stimulated if the position-dependent breakage parameter $\beta_3 < 0$ and erosion is stimulated if $\beta_3 > 0$. For this experiment, we used 30 equally spaced values for β_3:

$$\mathbf{B_3} = [-0.9, \dots, 10]$$

For the positional breakage parameter, it was expected that the higher the value, the more erosion will take place. This leads to a mechanism in which monomers on their own are more likely to be shed off the fibril. This leads to a general reduction in the number of fibrils. Hence, the polymer length distribution will flatten. Also, the polymer mass and concentration, mean length, breakage rate and R_0 will drastically reduce as a consequence of erosion. This is because monomers are the atomic units in this model. On the other hand, the center mechanism less likely leads to an excess of monomers to shed off. This will cause the length distribution to remain intact and the mean length and breakage rate to increase as well as R_0 and polymer mass and concentration. Furthermore, a lower (and negative) value for the position parameter leads to the opposite of the above.

The results are mostly in line with the hypotheses. From the simulation results, we get that a center mechanism promotes the sustainment of linear aggregates in the solution. This is seen by an increased

end-simulation aggregate concentration and mass for lower values of β_3 (**Figure 7A, B, C, D**). Furthermore, a center-breakage mechanism promotes the presence of on average shorter polymer lengths (**Figure 8A, B**). Lastly and importantly, the reproductive ratio was also influenced by β_3. To be precise, a center-breakage mechanism ($\beta_3 < 0$) promoted the proliferation of linear aggregates to a greater extent than erosion did ($\beta_3 > 0$) (**Figure 9**).

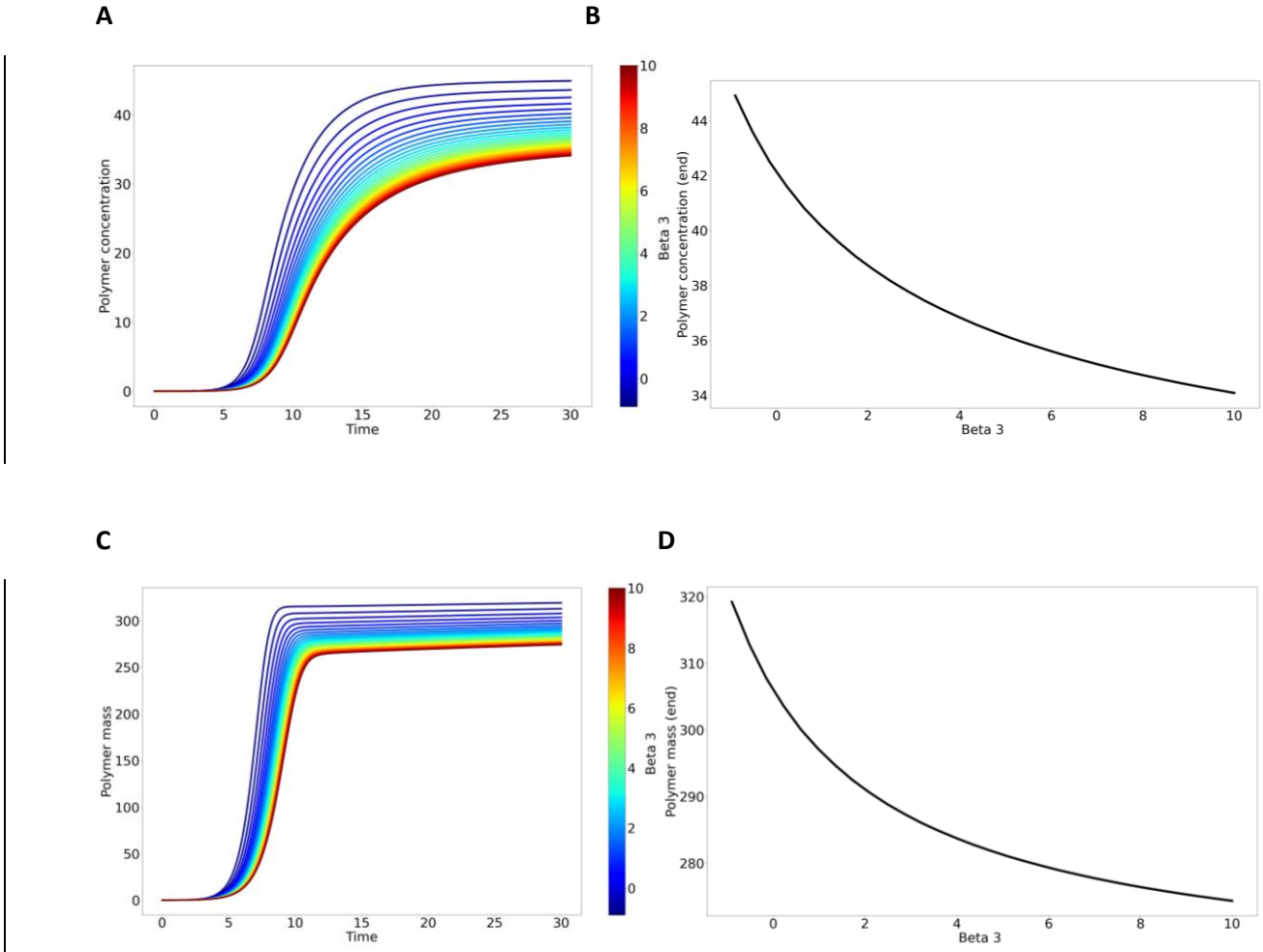

Figure 7. A) color plot of polymer aggregate concentration against time grouped by values of β_3, **B)** end-simulation polymer aggregate concentration plotted against β_3, **C)** color plot of polymer aggregate mass against time grouped by values of β_3, and **D)** end-simulation polymer aggregate mass plotted against β_3.

A **B**

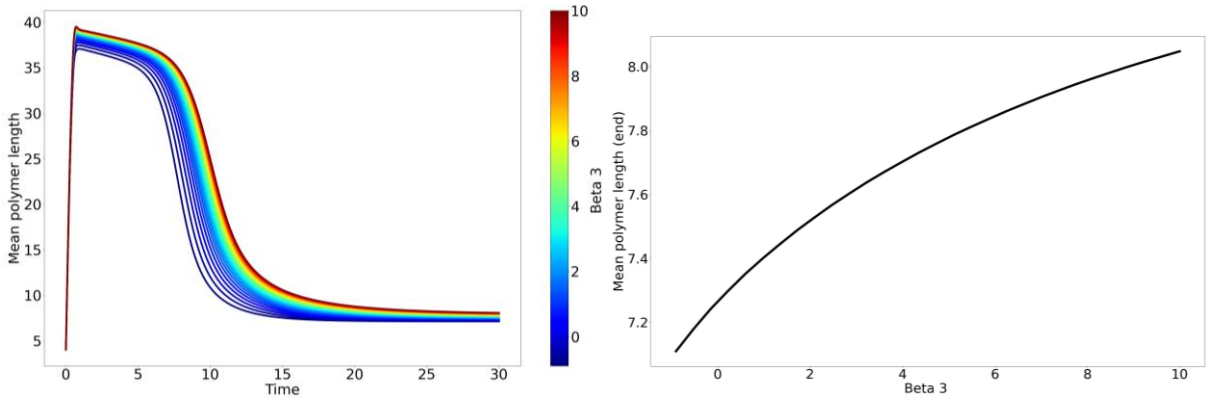

Figure 8. A) mean polymer length plotted against time grouped by β_3 and **B)** end-simulation mean polymer length plotted against β_3.

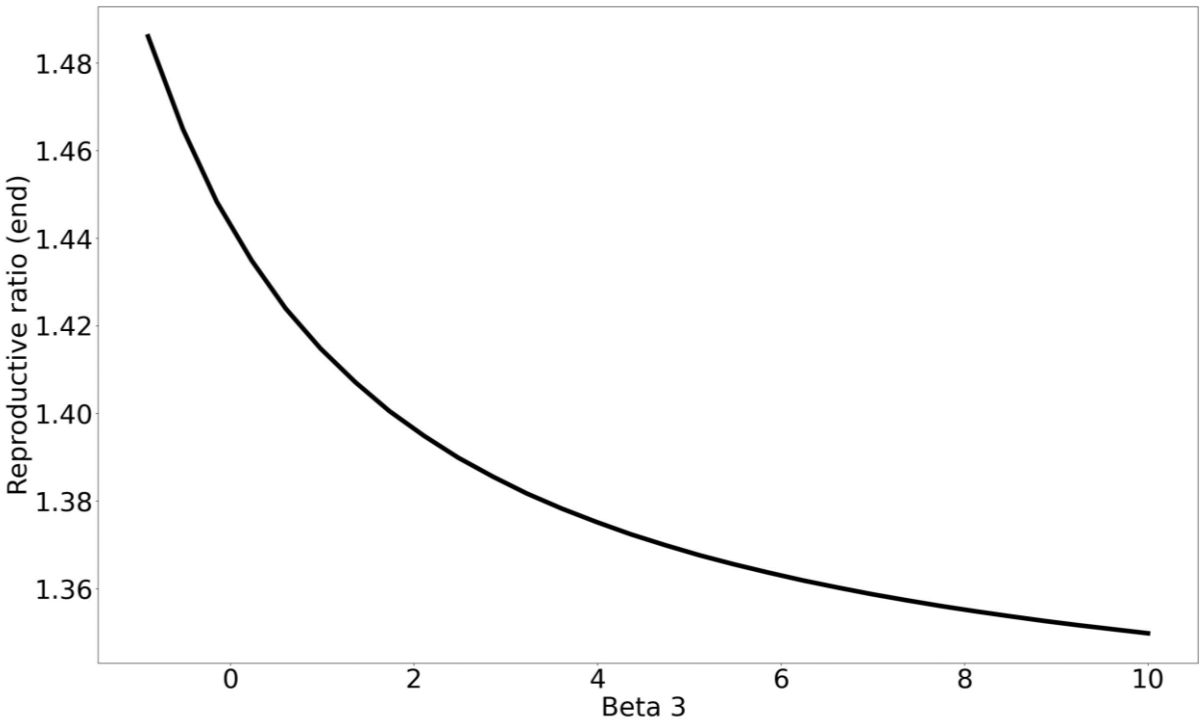

Figure 9. End-simulation reproductive ratio plotted against β_3.

Chaperones hamper elongation and breakage of linear protein aggregates

Chaperones are commonly known to refold misfolded proteins into more properly folded proteins. The following 30 equally spaced values for the chaperone dosage were used in the simulation experiment

$$\mathbf{D} = [0, \ldots 232]$$

In this simulation experiment, it turns out that chaperones hamper elongation by reducing the mean end-simulation length of the linear protein aggregates (**Figure 10A**). Furthermore, chaperones reduce

the breakage rate of protein aggregates (**Figure 10B**). The irregularity in the graphs of both figures may have been a matter of not simulating long enough.

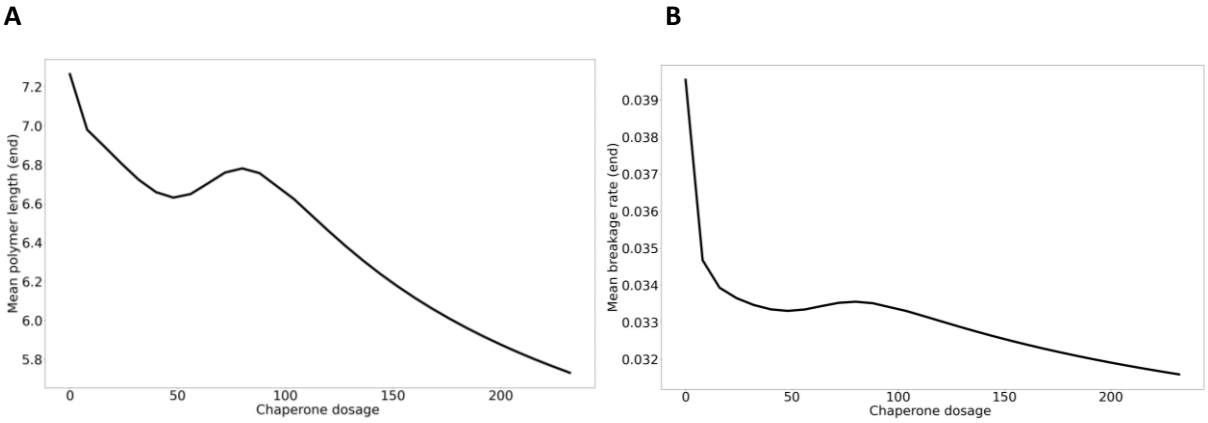

Figure 10. A) Mean end-simulation polymer length, and **B)** mean end-simulation breakage rate.

Interferons reduce reproductive capacity of linear protein aggregates in several ways

In this model, interferons are determined to directly degrade linear aggregates by the addition of an extra degradation term. Also here, 30 equally spaced values of interferons were chosen:

$$\mathbf{M_I} = [0, \dots, 1.45]$$

This resulted in a firm reduction of the end-simulation polymer mass for low doses and a complete abolishment of the latter for higher doses (**Figure 11A**). Furthermore, the infected free monomer concentration drops, whereas the healthy monomer concentration is partially preserved after the end-simulation time point (**Figure 11B, C**). Also, interferons drastically reduced the reproductive ratio of linear aggregates, thereby halting their propagation (**Figure 11D**).

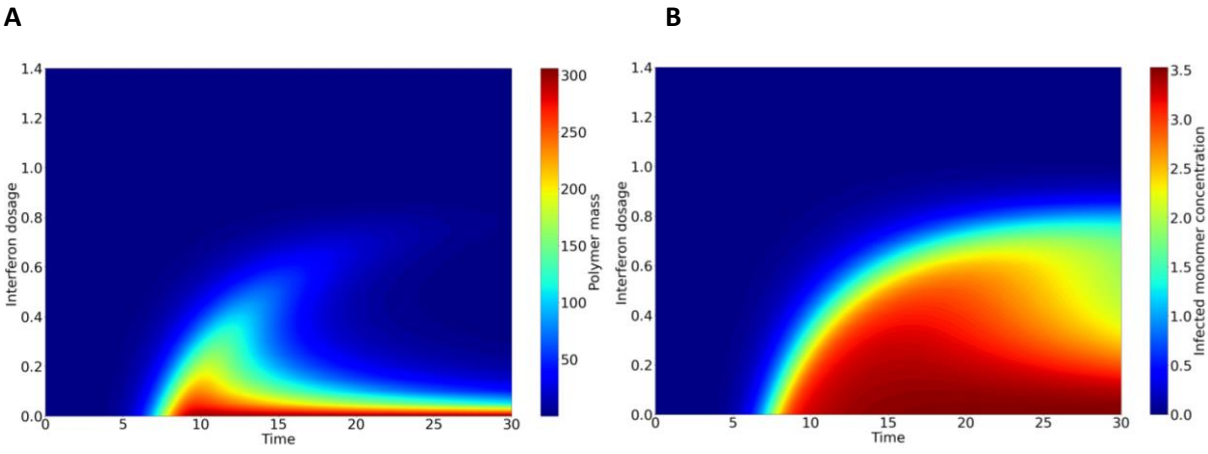

C **D**

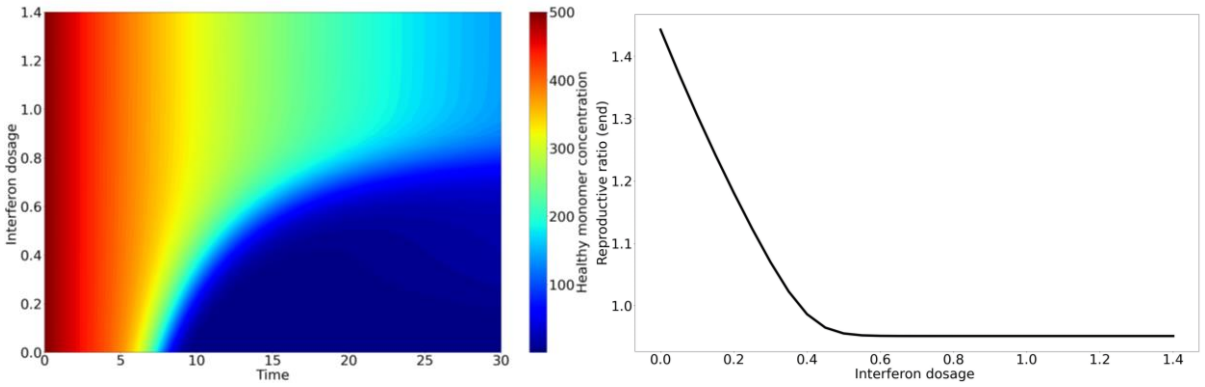

Figure 11. A) contour plot of total polymer mass, **B)** free infected monomer concentration, and **C)** healthy monomer concentration plotted against time and interferon dosage values. **D)** end-simulation reproductive ratio plotted against interferon dosage.

Part III – mediation analysis

In this part of the analysis, key parameters were varied in the way explained before, with a slight change for the range of β_2, namely $\mathbf{B_2} = [0, \dots, 1.7]$.

Length-dependent breakage decreases the critical treatment dose for chaperones but shows non-linearity in the same for interferons

The critical treatment dosage for any treatment option refers to the minimal dosage that causes the reproductive ratio to drop below 1. Hence, it is the lowest effective dosage. In general, we see that the end-reproductive ratio becomes more dependent on the chaperone dosage as β_2 increases (**Figure 12A**). Furthermore, the critical chaperone dosage drops drastically as β_2 increases (**Figure 12B**). An explanation of the above is that more monomers are released as β_2 is increased (see also **Figure 6C**). This makes the protein solution more receptive to chaperone-monomer association and hence more protection against further protein aggregation.

On the other hand, β_2 mediates the critical interferon dosage in a non-linear way. First, the critical dosage positively correlates with β_2, after which it drops for higher values of β_2 (**Figure 12A, B**). This result is inherent to the results obtained in **Figure 6B** and **Figure 6E**, where β_2 shows a negative parabolic relationship with total polymer mass and reproductive ratio. To summarize, for an intermediate value of β_2 it is harder for interferons to mitigate the infection if lengthy fibers are fragile enough to break easily (thus promoting infection propagate) without falling apart into unstable and noninfectious monomers (which hampers infection propagate).

A **B**

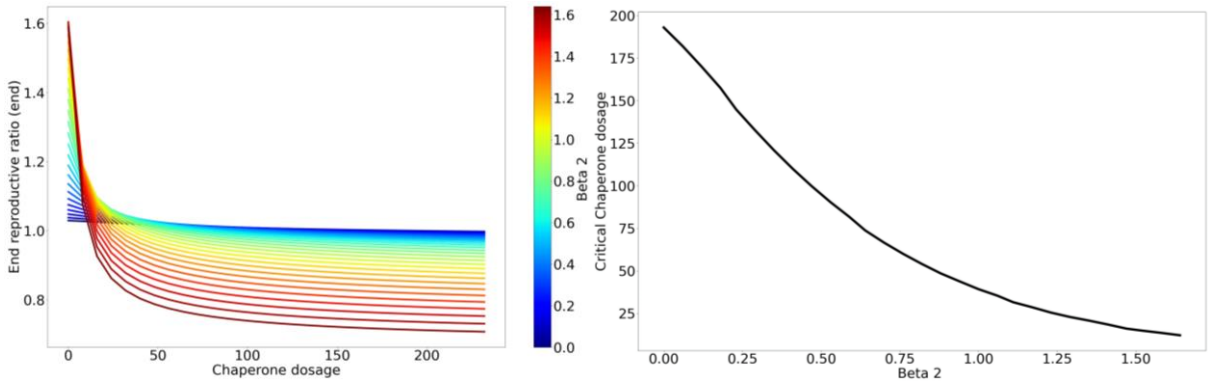

C **D**

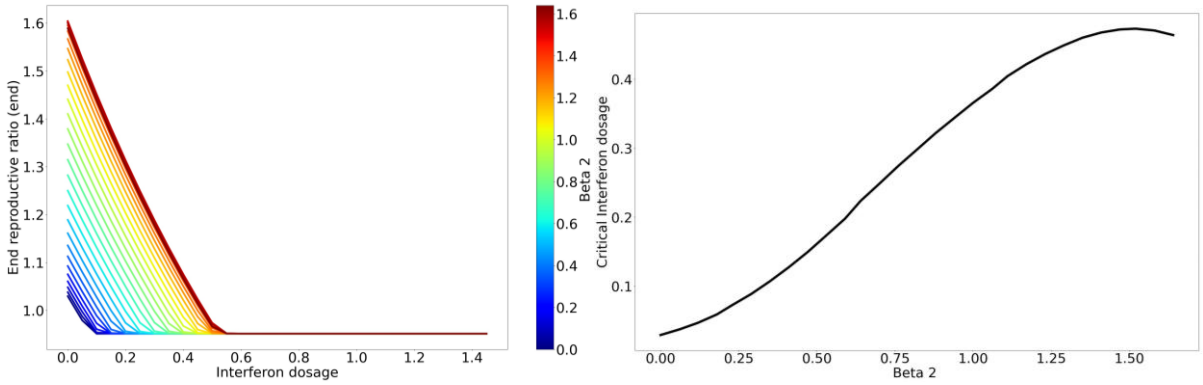

Figure 12. A) end-simulation value of the reproductive ratio plotted against chaperone dosage grouped by value of β_2, **B)** section of **A** at the point where the reproductive ratio equals 1. Critical chaperone dosage plotted against values of β_2. **C)** end-simulation reproductive ratio plotted against interferon dosage grouped by value of β_2. **D)** section of **C** at the point where the reproductive ratio equals 1. Critical chaperone dosage plotted against values of β_2.

Position-dependent breakage increases the critical treatment dose for chaperones but decrease the same for interferons

Here, we see that the relationship between the chaperone dosage and end-reproductive ratio is qualitatively the same for all value of β_3 (**Figure 13A**). However, when we look more closely at the result in **Figure 13B**, we see that there is a subtle increase in the chaperone dosage for the erosion mechanism. An explanation for this is that more misfolded monomers shed off from the linear aggregates during erosion. Hence, a higher chaperone dosage needs to be maintained to protect the many misfolded monomers from aggregating with polymers.

On the other hand, there was a subtle decrease in the critical interferon dosage for the erosion mechanism. This is also explained by the lower polymer concentration and mass as seen in **Figure 7A, B, C, D**.

A **B**

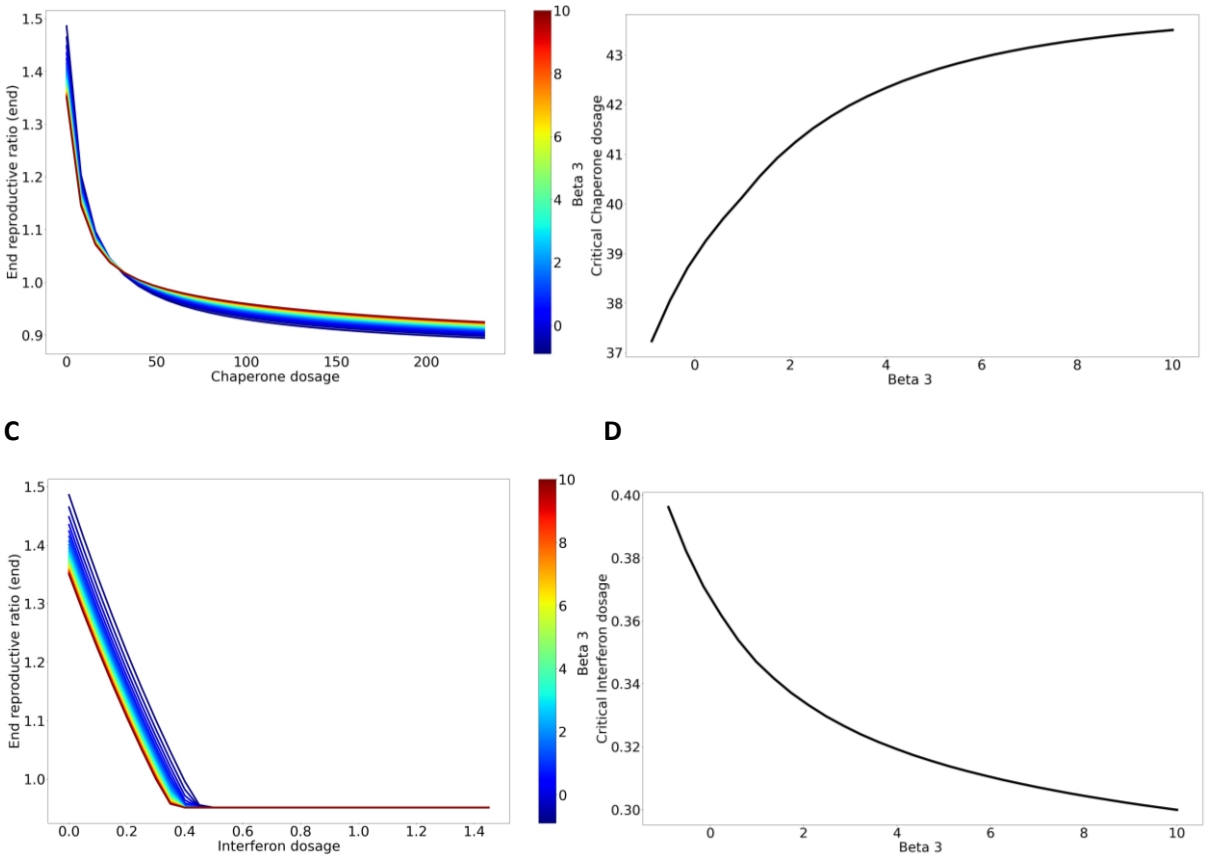

Figure 13. A) end-simulation value of the reproductive ratio plotted against chaperone dosage grouped by value of β_3, **B)** section of **A** at the point where the reproductive ratio equals 1. Critical chaperone dosage plotted against values of β_3. **C)** end-simulation reproductive ratio plotted against interferon dosage grouped by value of β_3. **D)** section of **C** at the point where the reproductive ratio equals 1. Critical chaperone dosage plotted against values of β_3.

Discussion

This work introduced two intrinsic fibril breakage parameters in combination with two treatment options. The intrinsic fibril breakage parameters were β_2; a length-dependent power law and β_3, a position-dependent parameter in a parabolic breakage kernel. The treatment options were chaperones or interferons. The results were obtained by means of differential equation modelling. We first looked at the validity of the model. After that, we performed an univariate analysis in which we varied only one of the four key parameters β_2, β_3, D, μ_I. Lastly, we performed a mediation analysis. Here, we looked at how the intrinsic breakage parameters mediate the effect of treatment regimens.

To begin with, both treatments individually and combined hampered the global propagation of linear protein aggregates, consistent with previous research on a similar model (Garzón et al., 2021). The basal dynamics of the model are in line with the hypotheses and with previous research. Monomers decayed according to a logistic decay curve (see also Shvadchak et al., 2015). Conversely, it could be shown that the population of the protein polymers over time followed a logistic growth curve (Alvarez-Martinez et al., 2011; Collins et al., 2004; Marchante et al., 2017; Nicoud et al., 2015; Xue & Radford, 2013). The evolution of the mean length over time was also similar in comparison to

previous research. To conclude, these findings do not seem surprising, as these are only qualitative patterns that are very likely to occur in similar models (Arioso, Beeg et al., 2012; Xue, Hellewell et al., 2009; Xue, Homans et al., 2009; Xue & Radford, 2013).

In general, it was shown that higher values of β_2 led to a faster accumulation of linear aggregates. Furthermore, β_2 imposed certain constraints on the length-distribution as well. This was seen by a more right-skewed length distribution of the linear aggregates. Next, β_2 determined the infectivity in a non-linear way. The latter has to do with optimal fragility. This means that long aggregates are fragile enough to break into shorter, infectious aggregates without being too fragile to break into non-infectious monomers. This was also reflected in the relationship between the critical interferon dose and β_2. For intermediate values of β_2, a relatively high amount of interferons was needed to halt the infection. On the other hand, the critical chaperone dosage dropped drastically as β_2 increased. One may conclude from this that manipulation of protein strains, such that they become more fragile (i.e. manipulate β_2) may be useful to inhibit protein aggregation. It is understandable that this is very hard, as protein aggregates are usually resistant to proteases. However, there is something that we did not incorporate into the model. This is that chaperones act as a fragilizing agent for protein aggregates as well. This does not seem to be a beneficial pathway, as fragmentation of protein aggregates promotes their propagation (see review of Kushnirov, Dergalev, & Alexandrov, 2021). Instead, it is of interest to stabilize protein aggregates, so that their propensity to break and propagate is reduced (a reduction in β_2). This can be achieved by protein sequestration. This is a method to prevent protein aggregates from breaking into smaller aggregates by binding of chaperones to the aggregate. In this way, propagation of aggregates can potentially be inhibited (Küffner et al., 2021). Hence, the results of the current protein propagation model are in agreement with and motivate concurrent clinical practice to inhibit protein aggregation.

Furthermore, the position-dependent breakage parameter showed its importance as well. To be precise, a center-breakage mechanism favors the propagation of linear protein aggregates. Also, linear aggregates on themselves tend to be shorter for the center-breakage mechanism, whereas monomers tend to increase in abundance for the erosion mechanism. The latter finding is consistent with earlier empirical findings of Beal and colleagues (2020). In future research, it might therefore be useful to stimulate erosion of protein aggregates rather than breakage at the center.

References

Abdelaziz, D. H., Abdulrahman, B. A., Gilch, S., & Schatzl, H. M. (2019). Autophagy pathways in the treatment of prion diseases. Current opinion in pharmacology, 44, 46-52. DOI: 10.1016/j.coph.2019.04.013.

Allen, K. D., Wegrzyn, R. D., Chernova, T. A., Müller, S., Newnam, G. P., Winslett, P. A., ... & Chernoff, Y. O. (2005). Hsp70 chaperones as modulators of prion life cycle: novel effects of Ssa and Ssb on the Saccharomyces cerevisiae prion [PSI+]. Genetics, 169(3), 1227-1242. DOI: 10.1534/genetics.104.037168.

Alvarez-Martinez, M. T., Fontes, P., Zomosa-Signoret, V., Arnaud, J. D., Hingant, E., Pujo-Menjouet, L., & Liautard, J. P. (2011). Dynamics of polymerization shed light on the mechanisms that lead to multiple amyloid structures of the prion protein. Biochimica et Biophysica Acta (BBA)-Proteins and Proteomics, 1814(10), 1305-1317. DOI: 10.1016/j.bbapap.2011.05.016.

Arosio, P., Beeg, M., Nicoud, L., & Morbidelli, M. (2012). Time evolution of amyloid fibril length distribution described by a population balance model. Chemical engineering science, 78, 21-32. DOI: 10.1016/j.ces.2012.04.031.

Arosio, P., Owczarz, M., Wu, H., Butté, A., & Morbidelli, M. (2012). End-to-end self-assembly of RADA 16-I nanofibrils in aqueous solutions. Biophysical journal, 102(7), 1617-1626. DOI: 10.1016/j.bpj.2012.03.012.

Baldwin, A. J., Anthony-Cahill, S. J., Knowles, T. P., Lippens, G., Christodoulou, J., Barker, P. D., & Dobson, C. M. (2008). Measurement of amyloid fibril length distributions by inclusion of rotational motion in solution NMR diffusion measurements. Angewandte Chemie, 120(18), 3433-3435. DOI: 10.1002/ange.200703915.

Balchin, D., Hayer-Hartl, M., & Hartl, F. U. (2016). In vivo aspects of protein folding and quality control. Science, 353(6294), aac4354. DOI: 10.1126/science.aac4354

Beal, D. M., Tournus, M., Marchante, R., Purton, T. J., Smith, D. P., Tuite, M. F., ... & Xue, W. F. (2020). The division of amyloid fibrils: Systematic comparison of fibril fragmentation stability by linking theory with experiments. Iscience, 23(9), 101512. DOI: 10.1016/j.isci.2020.101512.

Calvez, V., Lenuzza, N., Oelz, D., Deslys, J. P., Laurent, P., Mouthon, F., & Perthame, B. (2009). Size distribution dependence of prion aggregates infectivity. Mathematical biosciences, 217(1), 88-99. DOI: 10.1016/j.mbs.2008.10.007.

Calvez, V., Lenuzza, N., Doumic, M., Deslys, J. P., Mouthon, F., & Perthame, B. (2010). Prion dynamics with size dependency–strain phenomena. Journal of Biological Dynamics, 4(1), 28-42. DOI: 10.1080/17513750902935208.

Davis, J. K., & Sindi, S. S. (2015). A study in nucleated polymerization models of protein aggregation. Applied mathematics letters, 40, 97-101. DOI: 10.1016/j.aml.2014.09.007.

Engler, H., Prüss, J., & Webb, G. F. (2006). Analysis of a model for the dynamics of prions II. Journal of mathematical analysis and applications, 324(1), 98-117. DOI: 10.1016/j.jmaa.2005.11.021.

Eves, B. J., Doutch, J. J., Terry, A. E., Yin, H., Moulin, M., Haertlein, M., ... & Squires, A. M. (2021). Elongation rate and average length of amyloid fibrils in solution using isotope-labelled small-angle neutron scattering. RSC chemical biology, 2(4), 1232-1238. DOI: 10.1039/D1CB00001B.

Greer, M. L., Pujo-Menjouet, L., & Webb, G. F. (2006). A mathematical analysis of the dynamics of prion proliferation. Journal of theoretical biology, 242(3), 598-606. DOI: 10.1016/j.jtbi.2006.04.010.

Greer, M. L., van den Driessche, P., Wang, L., & Webb, G. F. (2007). Effects of general incidence and polymer joining on nucleated polymerization in a model of prion proliferation. SIAM Journal on Applied Mathematics, 68(1), 154-170. DOI: 10.1137/06066076X.

Igel-Egalon, A., Laferrière, F., Tixador, P., Moudjou, M., Herzog, L., Reine, F., ... & Béringue, V. (2020). Crossing species barriers relies on structurally distinct prion assemblies and their complementation. Molecular Neurobiology, 57, 2572-2587. DOI: 10.1007/s12035-020-01897-3.

Ionescu-Zanetti, C., Khurana, R., Gillespie, J. R., Petrick, J. S., Trabachino, L. C., Minert, L. J., ... & Fink, A. L. (1999). Monitoring the assembly of Ig light-chain amyloid fibrils by atomic force microscopy. Proceedings of the National Academy of Sciences, 96(23), 13175-13179. DOI: 10.1073/pnas.96.23.13175.

Ishibashi, D., Homma, T., Nakagaki, T., Fuse, T., Sano, K., Satoh, K., ... & Nishida, N. (2019). Type I interferon protects neurons from prions in in vivo models. Brain, 142(4), 1035-1050. DOI: 10.1093/brain/awz016.

Jin, T., Gu, Y., Zanusso, G., Sy, M., Kumar, A., Cohen, M., ... & Singh, N. (2000). The chaperone protein BiP binds to a mutant prion protein and mediates its degradation by the proteasome. Journal of Biological Chemistry, 275(49), 38699-38704. DOI: 10.1074/jbc.M005543200.

Kawahara, M., Kato-Negishi, M., & Tanaka, K. I. (2021). Neurometals in the pathogenesis of prion diseases. International Journal of Molecular Sciences, 22(3), 1267. DOI: 10.3390/ijms22031267.

Khurana, R., Ionescu-Zanetti, C., Pope, M., Li, J., Nielson, L., Ramírez-Alvarado, M., ... & Carter, S. A. (2003). A general model for amyloid fibril assembly based on morphological studies using atomic force microscopy. Biophysical journal, 85(2), 1135-1144. DOI: 10.1016/S0006-3495(03)74550-0.

Kim, C., Haldiman, T., Surewicz, K., Cohen, Y., Chen, W., Blevins, J., ... & Safar, J. G. (2012). Small protease sensitive oligomers of PrPSc in distinct human prions determine conversion rate of PrPC. DOI: 10.1371/journal.ppat.1002835.

Küffner, A. M., Linsenmeier, M., Grigolato, F., Prodan, M., Zuccarini, R., Palmiero, U. C., ... & Arosio, P. (2021). Sequestration within biomolecular condensates inhibits Aβ-42 amyloid formation. Chemical Science, 12(12), 4373-4382. DOI: 10.1039/d0sc04395h.

Kushnirov, V. V., Dergalev, A. A., & Alexandrov, A. I. (2021). Amyloid fragmentation and disaggregation in yeast and animals. Biomolecules, 11(12), 1884. DOI: 10.3390/biom11121884

Laferrière, F., Tixador, P., Moudjou, M., Chapuis, J., Sibille, P., Herzog, L., ... & Béringue, V. (2013). Quaternary structure of pathological prion protein as a determining factor of strain-specific prion replication dynamics. PLoS pathogens, 9(10), e1003702. DOI: 10.1371/journal.ppat.1003702.

Lu, J., Zhang, X., Wu, Y., Sheng, Y., Li, W., & Wang, W. (2021). Energy landscape remodeling mechanism of Hsp70-chaperone-accelerated protein folding. Biophysical Journal, 120(10), 1971-1983. DOI: 10.1016/j.bpj.2021.03.013.

Mankarious, S., Lee, M., Fischer, S., Pyun, K. H., Ochs, H. D., Oxelius, V. A., & Wedgwood, R. J. (1988). The half-lives of IgG subclasses and specific antibodies in patients with primary immunodeficiency who are receiving intravenously administered immunoglobulin. The Journal of laboratory and clinical medicine, 112(5), 634-640.

Marchante, R., Beal, D. M., Koloteva-Levine, N., Purton, T. J., Tuite, M. F., & Xue, W. F. (2017). The physical dimensions of amyloid aggregates control their infective potential as prion particles. Elife, 6, e27109. DOI: 10.7554/eLife.27109.

Masel, J., Jansen, V. A., & Nowak, M. A. (1999). Quantifying the kinetic parameters of prion replication. Biophysical chemistry, 77(2-3), 139-152. DOI: 10.1016/S0301-4622(99)00016-2.

Morris, R. J., Eden, K., Yarwood, R., Jourdain, L., Allen, R. J., & MacPhee, C. E. (2013). Mechanistic and environmental control of the prevalence and lifetime of amyloid oligomers. Nature communications, 4(1), 1891. DOI: 10.1038/ncomms2909.

Nichols, M. R., Moss, M. A., Reed, D. K., Lin, W. L., Mukhopadhyay, R., Hoh, J. H., & Rosenberry, T. L. (2002). Growth of β-amyloid (1− 40) protofibrils by monomer elongation and lateral association. Characterization of distinct products by light scattering and atomic force microscopy. Biochemistry, 41(19), 6115-6127. DOI: 10.1021/bi015985r.

Nicoud, L., Lazzari, S., Balderas Barragán, D., & Morbidelli, M. (2015). Fragmentation of amyloid fibrils occurs in preferential positions depending on the environmental conditions. The Journal of Physical Chemistry B, 119(13), 4644-4652. DOI: 10.1021/acs.jpcb.5b01160.

Nowak, M. A., Krakauer, D. C., Klug, A., & May, R. M. (1998). Prion infection dynamics. Integrative Biology: Issues, News, and Reviews: Published in Association with The Society for Integrative and Comparative Biology, 1(1), 3-15. DOI: 10.1002/(SICI)1520-6602(1998)1:1<3::AID-INBI2>3.0.CO;2-9.

Park, K. W., Eun Kim, G., Morales, R., Moda, F., Moreno-Gonzalez, I., Concha-Marambio, L., ... & Soto, C. (2017). The endoplasmic reticulum chaperone GRP78/BiP modulates prion propagation in vitro and in vivo. Scientific reports, 7(1), 44723. DOI: 10.1038/srep44723

Petrosyan, R., Patra, S., Rezajooei, N., Garen, C. R., & Woodside, M. T. (2021). Unfolded and intermediate states of PrP play a key role in the mechanism of action of an antiprion chaperone. Proceedings of the National Academy of Sciences, 118(9), e2010213118. DOI: 10.1073/pnas.2010213118.

Pieri, L., Madiona, K., & Melki, R. (2016). Structural and functional properties of prefibrillar α-synuclein oligomers. Scientific reports, 6(1), 1-15. DOI: 10.1038/srep24526

Prigent, S., Ballesta, A., Charles, F., Lenuzza, N., Gabriel, P., Tine, L. M., ... & Doumic, M. (2012). An efficient kinetic model for assemblies of amyloid fibrils and its application to polyglutamine aggregation. PloS one, 7(11), e43273. DOI: 10.1371/journal.pone.0043273.

Prigent, S., Haffaf, H. W., Banks, H. T., Hoffmann, M., Rezaei, H., & Doumic, M. (2014). Size distribution of amyloid brils. Mathematical models and experimental data. International Journal of Pure and Applied Mathematics, 93(6), 845-878. DOI: 10.12732/ijpam.v93i6.10.

Prüss, J., Pujo-Menjouet, L., Webb, G. F., & Zacher, R. (2006). Analysis of a model for the dynamics of prions. Discrete Contin. Dyn. Syst. Ser. B, 6(1), 225-235. DOI: 10.3934/dcdsb.2006.6.225.

Qiang, W., Kelley, K., & Tycko, R. (2013). Polymorph-specific kinetics and thermodynamics of β-amyloid fibril growth. Journal of the American Chemical Society, 135(18), 6860-6871. DOI: 10.1021/ja311963f.

Rubenstein, R., Gray, P. C., Cleland, T. J., Piltch, M. S., Hlavacek, W. S., Roberts, R. M., ... & Kim, J. I. (2007). Dynamics of the nucleated polymerization model of prion replication. Biophysical chemistry, 125(2-3), 360-367. DOI: 10.1016/j.bpc.2006.09.011.

Sakunthala, A., Datta, D., Navalkar, A., Gadhe, L., Kadu, P., Patel, K., ... & Maji, S. K. (2022). Direct demonstration of seed size-dependent α-synuclein amyloid amplification. The Journal of Physical Chemistry Letters, 13(28), 6427-6438. DOI: 10.1021/acs.jpclett.2c01650.

Shvadchak, V. V., Claessens, M. M., & Subramaniam, V. (2015). Fibril breaking accelerates α-synuclein fibrillization. The Journal of Physical Chemistry B, 119(5), 1912-1918. DOI: 10.1021/jp5111604.

Silveira, J. R., Raymond, G. J., Hughson, A. G., Race, R. E., Sim, V. L., Hayes, S. F., & Caughey, B. (2005). The most infectious prion protein particles. Nature, 437(7056), 257-261. DOI: 10.1038/nature03989.

Son, M., & Wickner, R. B. (2020). Normal levels of ribosome-associated chaperones cure two groups of [PSI+] prion variants. Proceedings of the National Academy of Sciences, 117(42), 26298-26306. DOI: 10.1073/pnas.2016954117.

Sorci, M., Grassucci, R. A., Hahn, I., Frank, J., & Belfort, G. (2009). Time-dependent insulin oligomer reaction pathway prior to fibril formation: Cooling and seeding. Proteins: Structure, Function, and Bioinformatics, 77(1), 62-73. DOI: 10.1002/prot.22417.

Sorci, M., Silkworth, W., Gehan, T., & Belfort, G. (2011). Evaluating nuclei concentration in amyloid fibrillation reactions using back-calculation approach. Plos one, 6(5), e20072. DOI: 10.1371/journal.pone.0020072.

Tanaka, M., Collins, S. R., Toyama, B. H., & Weissman, J. S. (2006). The physical basis of how prion conformations determine strain phenotypes. Nature, 442(7102), 585-589. DOI: 10.1038/nature04922.

Tarutani, A., Suzuki, G., Shimozawa, A., Nonaka, T., Akiyama, H., Hisanaga, S. I., & Hasegawa, M. (2016). The effect of fragmented pathogenic α-synuclein seeds on prion-like propagation. Journal of Biological Chemistry, 291(36), 18675-18688. DOI: 10.1074/jbc.M116.734707.

Tixador, P., Herzog, L., Reine, F., Jaumain, E., Chapuis, J., Le Dur, A., ... & Beringue, V. (2010). The physical relationship between infectivity and prion protein aggregates is strain-dependent. PLoS pathogens, 6(4), e1000859. DOI: 10.1371/journal.ppat.1000859.

Tzaban, S., Friedlander, G., Schonberger, O., Horonchik, L., Yedidia, Y., Shaked, G., ... & Taraboulos, A. (2002). Protease-sensitive scrapie prion protein in aggregates of heterogeneous sizes. Biochemistry, 41(42), 12868-12875. DOI: 10.1021/bi025958g.

Van Raaij, M. E., Van Gestel, J., Segers-Nolten, I. M., De Leeuw, S. W., & Subramaniam, V. (2008). Concentration dependence of α-synuclein fibril length assessed by quantitative atomic force microscopy and statistical-mechanical theory. Biophysical journal, 95(10), 4871-4878. DOI: 10.1529/biophysj.107.127464.

Wu, K., Stull, F., Lee, C., & Bardwell, J. C. (2019). Protein folding while chaperone bound is dependent on weak interactions. Nature Communications, 10(1), 4833. DOI: 10.1038/s41467-019-12774-6.

Wyszkowski, H., Janta, A., Sztangierska, W., Obuchowski, I., Chamera, T., Kłosowska, A., & Liberek, K. (2021). Class-specific interactions between Sis1 J-domain protein and Hsp70 chaperone potentiate disaggregation of misfolded proteins. Proceedings of the National Academy of Sciences, 118(49), e2108163118. DOI: 10.1073/pnas.2108163118.

Xue, W. F., Hellewell, A. L., Gosal, W. S., Homans, S. W., Hewitt, E. W., & Radford, S. E. (2009). Fibril Fragmentation Enhances Amyloid Cytotoxicity* ◆. Journal of Biological Chemistry, 284(49), 34272-34282. DOI: 10.1074/jbc.M109.049809.

Xue, W. F., Homans, S. W., & Radford, S. E. (2009). Amyloid fibril length distribution quantified by atomic force microscopy single-particle image analysis. Protein Engineering, Design & Selection, 22(8), 489-496. DOI: 10.1093/protein/gzp026.

Xue, W. F., Hellewell, A. L., Hewitt, E. W., & Radford, S. E. (2010). Fibril fragmentation in amyloid assembly and cytotoxicity: when size matters. Prion, 4(1), 20-25. DOI: 10.4161/pri.4.1.11378.

Xue, W. F., & Radford, S. E. (2013). An imaging and systems modeling approach to fibril breakage enables prediction of amyloid behavior. Biophysical journal, 105(12), 2811-2819. DOI: 10.1016/j.bpj.2013.10.034.

Zimmermann, M. R., Bera, S. C., Meisl, G., Dasadhikari, S., Ghosh, S., Linse, S., ... & Knowles, T. P. (2021). Mechanism of secondary nucleation at the single fibril level from direct observations of Aβ42

aggregation. Journal of the American Chemical Society, 143(40), 16621-16629. DOI: 10.1021/jacs.1c07228.

Supplementary information

Supplementary figures

A

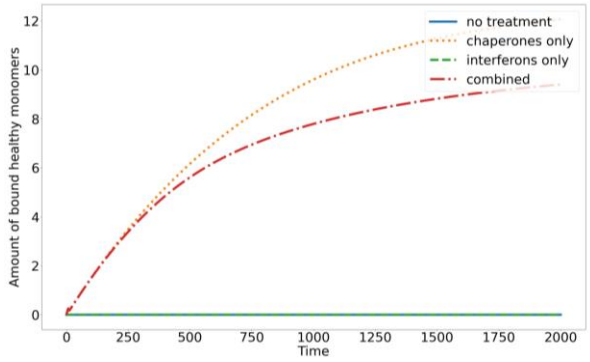

B

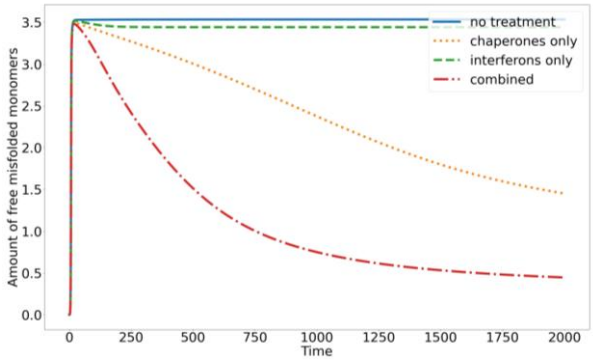

C

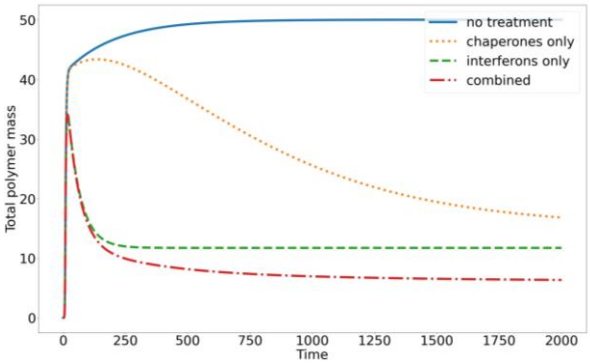

Supplementary figure 1. A) The amount of monomers bound to chaperones and **B)** the amount of misfolded monomers and **C)** The total polymer mass plotted against time for each treatment option. Relevant parameter settings are, in respective order: $(D, \mu_I) = \{(0,0), (0.040,0), (0,0.015), (0.040,0.015)\}$. Other parameter settings: $n = 4; \lambda = 2; \alpha_M = 0.02; \alpha_R = 0.4; \delta_M = 0.4; \delta_R = 0.02; \phi_M = 0.4; \mu_C = 0.001; \mu_M = 0.05; \mu_R = 0.05; \mu_P = 0.005; \varepsilon = 0.16; \beta_1 = 0.04; \beta_2 = 1;\ \beta_3 = 0$. Initial conditions were $M(0) = 500$, $P_{n\to 4}(0) = 0.001$ and all other initial values were set at 0. In case R_0 was calculated, the initial healthy equilibrium conditions were $M(0) = \frac{\lambda}{\mu_M}$, $C(0) = \frac{D}{\mu_C}$.

A **B**

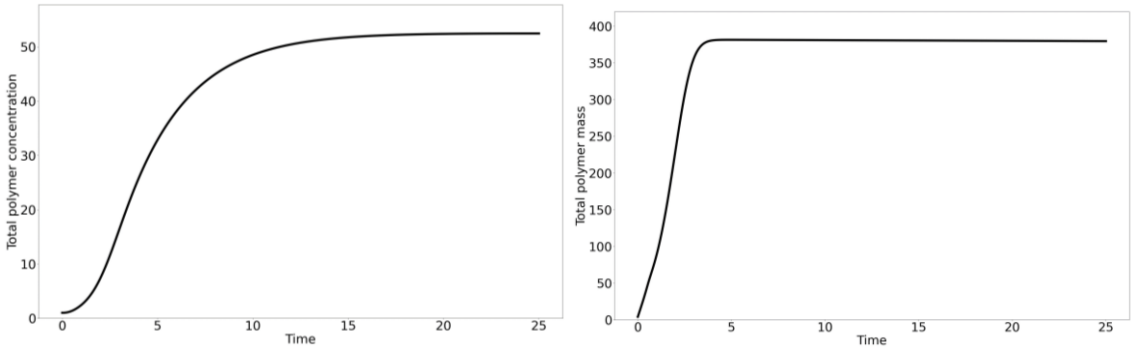

Supplementary figure 2. A) The polymer concentration and **B)** mass plotted against time. Here, the only difference is the initial condition $P_{n\to 4}(0) = 1$.

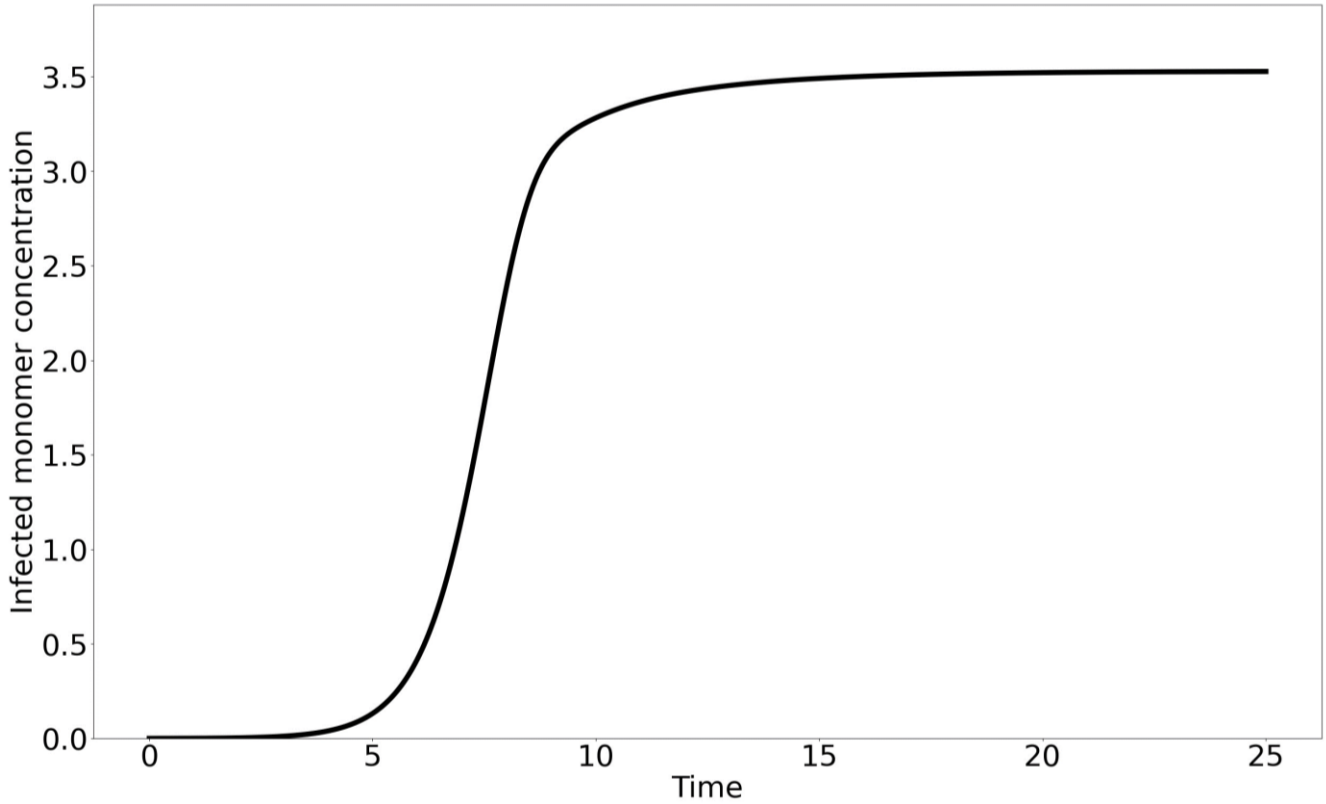

Supplementary figure 3. Plot of the free infected monomer concentration.

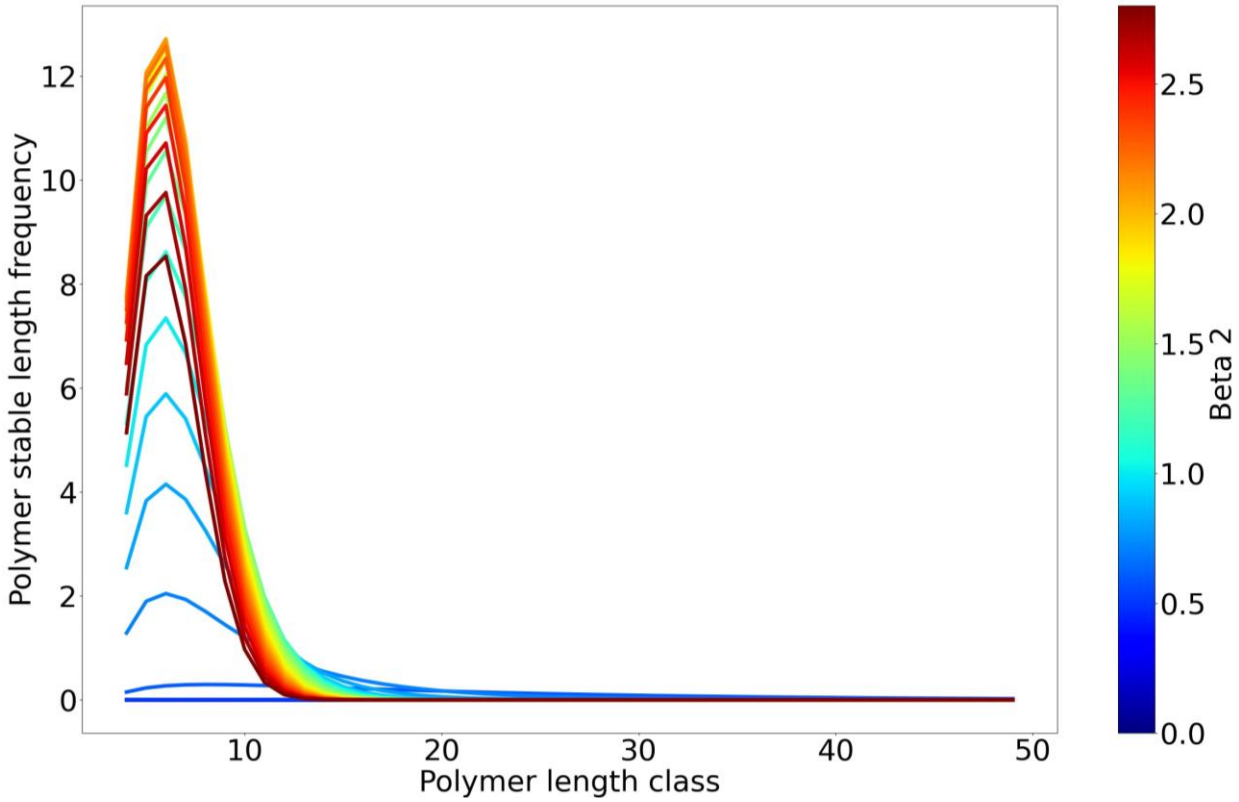

Supplementary figure 4. The stable length distribution of polymer lengths. The coloring of the lines depend on the value of β_2.